University of Pécs
Doctoral School of Chemistry

The effect of the geometric variability of the stationary phase on the peak shape in liquid chromatography

PhD thesis

Annamária Sepsey

Supervisor:
Dr. Attila Felinger
professor of chemistry

Pécs, 2016

Contents

1

Motivation and Problem Statement

> *It was a wild and stormy night on the West Coast of Scotland. This, however, is immaterial to the present story, as the scene is not laid in the West of Scotland. For the matter of that the weather was just as bad on the East Coast of Ireland.*
>
> — **Stephen Leacock**

The efficiency of the chromatographic separations is decisively affected by the physical parameters of the column and the sample molecules, such as the pore size and distribution of the stationary phase and the molecule size and distribution of the sample. The most preferred method to investigate the relative size of the sample molecules to the pores is Size Exclusion Chromatography (SEC). It allows to get a more accurate picture of the impact of the distributions on the separation because in an ideal case there is no interaction between the sample molecules and the stationary phase, the separation is only based on the size of the molecule relative to the pore size. To take these effects into account however, a proper model is needed which comprises the above mentioned distributions. The stochastic theory of chromatography provides an appropriate tool to investigate the separation process at a molecular level and allows considering the heterogeneity of the pore sizes and the polymer polydispersion.

The main aims of this work were:

- integration of the pore size distribution into the stochastic theory of chromatography to obtain the characteristic function and main moments describing the chromatographic peak;
- investigation of the effects of the parameters influencing on the separation by taking into account the possible pore geometries;

- determination of the porous structure (pore size distribution and pore geometry) of commercially available columns filled with totally porous and superficially porous particles using the novel model;
- investigation of the difference in the porous structure of commercially available silica-based monolithic columns of the first and second generations using the novel model;
- integration of the molecule size distribution (polydispersity) into the stochastic theory of chromatography to investigate the effect of that on the separation and its efficiency for various pore geometries.

We first give a short overview about the stationary phases most often used in analytical liquid chromatographic practice and the main band broadening factors, the emergence of the chromatographic peak. Further on we introduce the main aspects of size exclusion chromatography and its stochastic theory. In the second part, the result of our work is presented. After the derivation of the novel stochastic model containing the pore size distribution, we demonstrate the effects of the parameters influencing the chromatographic separation. The derived model is used to determine the pore geometry and the pore size distribution of several chromatographic columns with different structures. We also investigate the effect of the polydispersity by integrating the distribution of the molecule size into the stochastic theory of size exclusion chromatography and demonstrate the effects caused by those parameters on the separation.

2 Literature review

> *Not everything that can be counted counts.*
> *Not everything that counts can be counted.*
>
> — **William Bruce Cameron**

2.1 Column technology

Column packings in High Performance Liquid Chromatography (HPLC) are usually filled in a metal or plastic cylindrical tube and consist of a rigid support and in most cases an attached stationary phase. Based on the morphology of the support material, we can distinguish columns where the separation takes place on the surface area of spherical particles and columns where the analyte wanders through a single monolithic mesh. A monolith may be thought of as one big rigid sponge that fills the entire column and composed of an interconnected, porous bed. The emergence of monolithic columns offers a great alternative, however the most frequently used chromatographic columns are packed with small spherical particles. The size of these particles can be in various ranges, but the nowadays typically used analytical columns are packed with particles of ca. 3 µm mainly as a means for decreasing run time and increasing sample throughput. Recently narrow-bore columns packed with sub–2 µm particles have been introduced for Ultra-High Performance Liquid Chromatography (UHPLC) measurements.

The structure of the support material is of main importance because the interaction between the sample molecules and the stationary phase occurs on the interface region of the bed. Both the spherical and monolithic adsorbents are of high surface area which is provided by their porous interface, thus very efficient separations can be achieved with them. For SEC, the specific pore volume is very important, since this is where the separation takes place. If

all other things are equal, a larger pore volume results in a better separation. For retention chromatography, the pore volume however is only a necessary evil, providing access to the internal surface. The surface area within the pores of the particle is responsible for retention, and the surface area per column volume (i.e. the phase-ratio) is a measure of the retentivity of the material.

The support material is mainly synthesized from porous silica based on its good physico-chemical properties such as rigidity, pH, mechanical stability, manufacturability and reproducibility. Besides silica, other inorganic materials (alumina, titania, zirconia, porous carbon), organic polymers (acrylamides, styrene divinylbenzene, methacrylates, saccharides and vinyl-alcohols) and silica-organo hybrids are also used, mainly for special tasks [1]. The surface modification of the support material is chemically made as needed based on the retention method. The most commonly used modifications are still C_8 and C_{18}.

Several particle configurations are currently available for HPLC. Based on the degree of porosity, we can distinguish three types of spherical particles: nonporous, totally porous and superficially porous particles. As mentioned before, a novel group of stationary phases is represented by the monoliths.

2.1.1 Nonporous particles

The surface area of the nonporous particles equals to the geometrical surface of the spheres. Due to the lack of pores, rapid separations with excellent recoveries can be obtained [2, 3]. The column's loadability however is usually low and the pressure drop is high while using columns packed with nonporous particles. The general application of these columns is nevertheless only recommended for macromolecules and large biomolecules [4, 5].

The separation becomes usually more effective as the surface of the solid phase increases, eg. using porous support materials.

2.1.2 Porous particles

Most particles used in HPLC are porous and have high specific surface area and pore volume. There are two types of porous stationary phase particles

used in liquid chromatography practice: totally porous particles (TPP) and superficially porous particles (SPP) (also called pellicular, fused-core, core-shell or controlled-surface-porosity particles). Both of them have much greater surface areas than nonporous particles. The only difference is that the latter particles have a solid core and the porous layer of desired thickness is syntesized around this core as a shell. The more realistic view of this structure is that the porous part is formed as layers of little porous colloidal particle aggregates which form diffusive pores with pore diameters of 8 to 30 nm.

Fig. 2.1 shows transmission electron microscopy (TEM) and scanning electron microscopy (SEM) photos showing the structure and the surface of a core-shell particle. The use of these core-shell particles results in fast and highly efficient separations and high peak capacities due to the shorter diffusion path length and quick mass-transfer inside the porous layer.

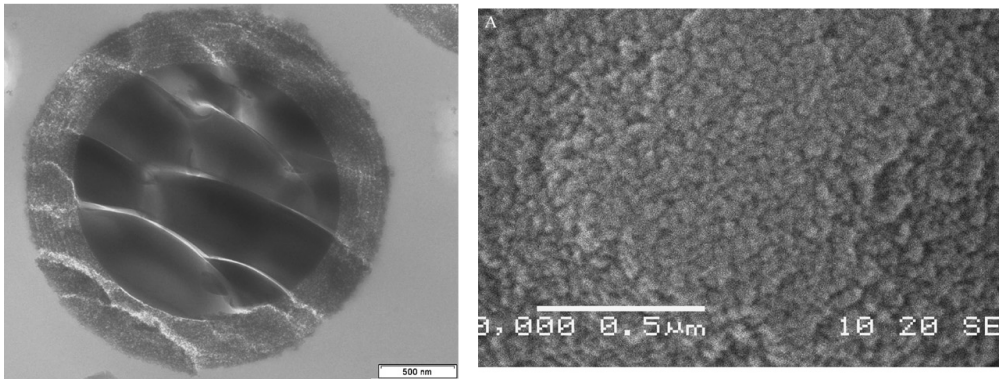

Fig. 2.1: Left: TEM photograph of the cut of a 2.6 µm Kinetex core-shell particle (SPP). Right: SEM photograph at the surface of a 2.6 µm Kinetex particle [6].

Totally porous particles were the most commonly used until the more efficient superficially porous particles were commercialized in the late 2000s. They have diameters in the 1.5–5 µm range and are prepared by the aggregates of small spheres which form the pores.

Due to the larger surface, TPPs are of greater column capacity but is several cases also of lower efficiency compared to the equal sized SPPs. Although the size of the TPPs could be decreased in order to increase the separation efficiency, this would result in a significant increase in pressure drop and temperature gradients which should be avoided. Columns packed with SPPs having diameter of 2.7 µm (1.7 µm solid core covered by 0.5 µm thick shell) achieved the same or better efficiencies than columns packed with 1.7 µm

TPPs with the additional advantage of operating at back pressures that are two or three times lower [7].

The study of the pore structure of the stationary phases used in liquid chromatography has been of great interest among experts in the last decades [8–11]. The porous particles are characterized by mainly three parameters: the specific surface area, the specific pore volume, and the pore diameter. These values strongly influence each other and also other circumstances that should be considered while optimizing the separations:

- the pore diameter has to be large enough to allow the solvated analyte to access the internal surface of the pores by diffusion to achieve an interaction;
- the larger the pore diameter, the less the specific surface area will be;
- retention increases while decreasing the pore size (and thus increasing the surface area);
- the maximum amount of sample that can be injected is proportional to surface area thus the smallest possible pore diameter is suggested to use;
- solute molecules must be able to enter the pores without hindrance which requires as a rule of thumb eight times larger pores than the solute molecules [12], and
- as particle size is decreased, the pressure drop increases.

The nature of the pores depends to some degree on the method used to synthesize the particles. Except for some special cases, the internal structure is homogeneous throughout the particle. Based on their diameters, pores are classified by International Union of Pure and Applied Chemistry (IUPAC) [13] as follows:

- micropores: less than 2 nm,
- mesopores: intermediate range (between 2 and 50 nm),
- macropores: exceeding 50 nm.

The micropore range can be further subdivided into micropores and submicropores, the latter having a diameter less than 1 nm, but this borderline is not yet fully defined [14].

The pore shape or geometry is also an important feature because if the analyte molecules cannot diffuse through the pores, the separation is hindered. The mostly assumed pore shapes are: slits, cylinders, and cones or spheres.

2.1.3 Monolithic phases

Monolithic columns were introduced in the late 1980s and from that time they have received increasing attention [15–22]. They can be visualized as a single, continuous network and can be made either from porous silica or by the co-polymerization of monomers such as styrene/divinylbenzene with vinyl/divinyl methacrylate. This novel bed structure with large macropores and small mesopores allows highly efficient analyses due to rapid mass transfer [22, 23]. The resulting surface area is contributed mainly by the mesopores, while flow through the column occurs in the macropores. In monolithic beds the macropores (also called flow-through pores) are much larger than the skeleton thickness, and the size of solid and void elements and their size statistics do not strictly depend on each other.

The great advantage of monoliths is their permeability, so that the required operational pressure is much less than it is for conventional packed bed columns. Because of their higher external porosity, higher flow rates can also be used without a corresponding loss in column efficiency. Another essential feature of monolithic columns is that they require no frit systems at the column inlet and outlet which would cause extra band-broadening. Their void volume can reach as high as 80%. The pore structure permits the separation of proteins, oligonucleotides, nanoparticles (DNA, RNA) and even living organisms (viruses, bacteria) [24].

The first monolithic column was introduced in 2000 as Chromolith Performance by Merck. It was a 100 mm×4.6 mm cylindrical rod sealed with a polyether ether ketone (PEEK) tube. Its bimodal porous network consists of macropores of 2 μm which provides high permeability and mesopores of 13 μm which ensures the large specific surface area. The monolithic columns marketed till 2011 were members of the first generation monoliths (1G).

Despite the great efficiency shown by the 1G columns, some important limiting factors were shown [25–27] in connection with the morphology of these monoliths:

- the random geometry (pore size and spatial distribution) and large domain size leads to a loss in efficiency;
- the irregularities on the surface of the porous silica skeleton lead to higher film mass transfer resistance, and

- the radially heterogeneous morphology introduces a mobile phase velocity bias between the local regions of the column cross-section leading to band-broadening and tailing of the peaks.

The second generation monoliths (2G) were introduced in 2011 as Chromolith HighResolution columns where the domain size was decreased by ca. 30–35% and radial heterogeneity of the macroporosity distribution was eliminated, which substantially decreases transcolumn dispersion [25, 28]. Fig. 2.2 shows pictures obtained by SEM for both generations of monolith showing structural differences at 2000:1 and 5000:1 magnifications.

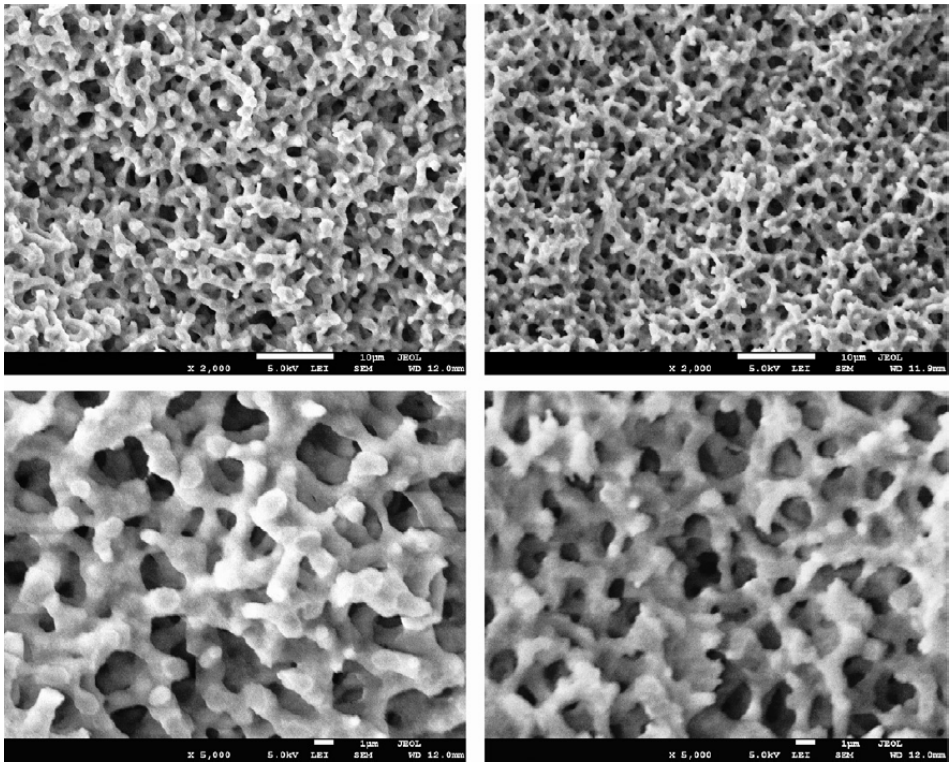

Fig. 2.2: SEM images of bare-silica rods (4.6 mm × 150 mm) from the 1st (left) and 2nd (right) Chromolith generation at 2000:1 (top) and 5000:1 (bottom) magnification [29].

The more homogeneous macropore space at the short-range interchannel scale has brought a remarkable improved separation efficiency at unchanged retention properties which has been evaluated for analysis of both small molecules and large biomolecules [27, 29–32]. The result is 66.5% reduction of the minimum plate height, compared to the 1G monoliths [29].

2.2 Band broadening processes in liquid chromatography

In chromatography the sample components become distributed over the separation path as discrete zones and these zones expand continuously as the separation process advances. The result of the separation depends on whether the zones are narrow enough so that we can keep avoiding overlap and cross contamination with adjacent zones [33]. Therefore the major aim in chromatography is the limitation of zone spreading. To fulfill this, one needs to understand the processes underlying the zone formation and spreading.

The events contributing to zone spreading in separation systems are of a random nature. The central limit theorem of statistics guarantees that a sequence of random events of the most general kind will lead to a Gaussian distribution function if the single random displacements are independent and small compared to the final mean displacement [34]. If this is fulfilled, the variances of the independent processes (σ_i^2) contributing to the zone spreading are additive. Thus the total variance can be written as

$$\sigma_\mathrm{total}^2 = \sigma_1^2 + \sigma_2^2 + \sigma_3^2 + \cdots = \sum_{i=1}^{n} \sigma_\mathrm{i}^2. \tag{2.1}$$

Since the apparent diffusion coefficients (D_i) are directly proportional to the respective variances and inversely proportional to the time (t) as

$$D_\mathrm{i} = \frac{\sigma_\mathrm{i}^2}{2t}, \tag{2.2}$$

they are additive in the same manner ($D_\mathrm{total} = \sum D_\mathrm{i}$). With each increment in zone spreading there is obviously a corresponding loss of separation efficiency. Fig. 2.3 illustrates the contributions to overall band spreading obtainable in a chromatographic system.

The spreading caused by the HPLC system (injection needle, needle seat capillary, injection valve, connecting tubes, detector cell [35]) and column hardware can be measured and optimized easily. The dead volume contains only these effects and we can remove them the easiest way by deconvolution of an inert, unretained component's peak from the analyte's peak we are interested in. By this operation – which is also called as normalization to

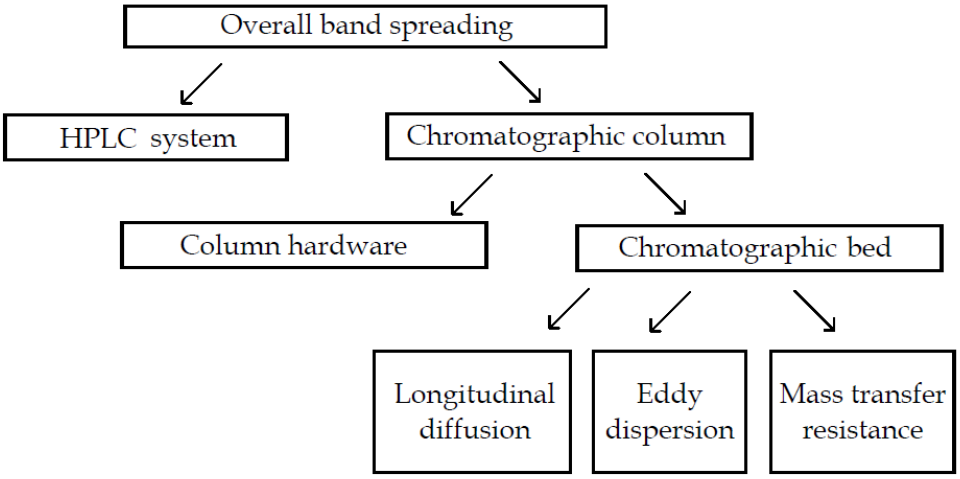

Fig. 2.3: Contributions to overall band spreading in a chromatographic system

thy system volume –, we achieved that the initial zone of the analyte can be approximated at relative low concentrations as a Dirac delta function, which is an infinitely narrow zone of unit area. The diffusion and diffusion-like processes in the column convert even such a delta function to a Gaussian one with the passage of time (Fig. 2.4a). However if the initial zone was already Gaussian, it becomes broader and lower as time passes (Fig. 2.4b). If the initial zone cannot be approximated by a delta function, the final zone can be obtained as a sum of Gaussian functions [33].

In the bed while separating the components from each other, several processes occur: the analyte molecules travel with the mobile phase along the column at high pressure while several adsorption/desorption steps occur. We can distuinguish three major sources of zone dispersion inside the chromatographic bed [36, 37]:

- longitudinal diffusion along the mobile phase percolating through the bed, which is inversely proportional to the mobile phase velocity since the lesser time the band spends in the column, the lesser time it has to diffuse;
- multipath (eddy) dispersion, due to the anastomosis of the channels conveying the sample band across the bed of particles;
- mass transfer resistance, due to the time molecules need to diffuse in and out of the particles and through their pores and due to slow adsorption-desorption kinetics.

These three contributions account for the band broadening due to the mass transfer processes encountered in any type of chromatographic column

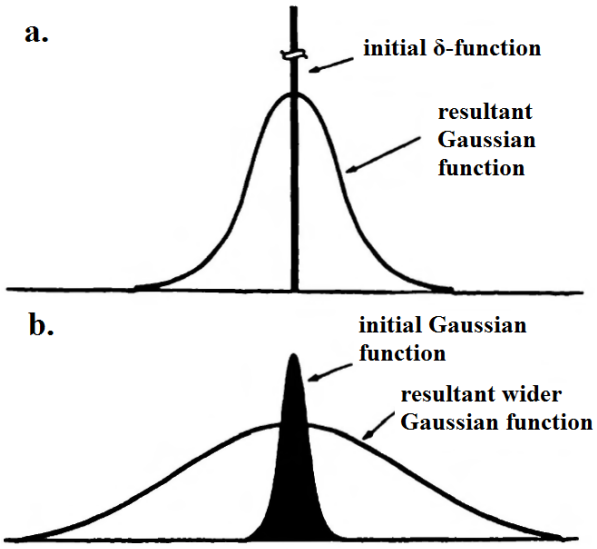

Fig. 2.4: Formation of concentration profiles depending on the shape of the initial profile [33]

(packed, or monolithic columns), independent of the physical state of the mobile phase (gas, liquid, or supercritical fluid), the flow regime (laminar to turbulent), or the nature of the stationary phase (liquid, solid, or narrow pores where molecular movements are hindered) [38].

2.3 Distributions contributing to band broadening

In the previous chapter, the classical, long known peak broadening factors were discussed. However, other contributions can also affect the peak shape and thus separation efficiency. In this section the distributions of the stationary phase particles and the distribution of the molecule size affecting the separation efficiency will be discussed. Others such as temperature-induced effects won't be addressed.

2.3.1 Particle size distribution

The physical characteristics of particles are important and manufacturers monitor the particle properties in various ways. The size of the particles is especially important, as this largely determines the size of the channels between particles and thus the efficiency of the packed column. However, the particle size cannot be defined by a single value, it is governed by a distribution that may cover a wide range [39]. The particle size and its

distribution can be obtained either with electron microscopy, or with special instruments such as Coulter counter which provide more convenient and quantitative information. The typical relative standard deviation of the particle size is 5% for superficially porous particles and 10–20% for totally porous particles but it strongly depends on the method used to characterize it [40].

The importance of particle diameter in influencing separation has been discussed several times in practice and by chromatographic models as well [39, 41–48]. There are several contradictory consequences that were drawn on the efficiency of the separations. According to one of the most recent papers published which is in good agreement with measured data, there is no evident correlation between the particle size distribution and column efficiency [47]. Beside this, a narrow particle size distribution provides lower pressure drop for comparable efficiency.

2.3.2 Pore size distribution

As demonstrated in Section 2.1.2, porous particles can be characterized also by their specific surface area, specific pore volume and pore diameter which depend strongly on each other. The pores provide the surface area neccesary for separations in adsorption or partition chromatography and the molecules are separated according their size relative to that of the pore diameter's in SEC. The pore diameter, however – similarly to the particle size – is not a constant, well-definable value, the pores of modern porous stationary phase may exhibit a momentous pore size distribution (PSD) which is an important feature of the adsorbent [13]. Experimental data confirm that the size of pores can cover a rather wide range including pores in the molecular size range as well as macroscopic fissures and cracks thus the pore size should preferably be presented on a logarithmic scale [39, 49]. This is shown in Fig. 2.5.

The nature and the breadth of the PSD have significant impact on the mass-transfer properties of the stationary phase thus on the efficiency of the separation, since the hindered diffusion of the molecules in the pore network gives a critical contribution to band broadening.

There are a number of methods for determining relevant information about the porous media. Particle surface-area and PSD typically are measured by

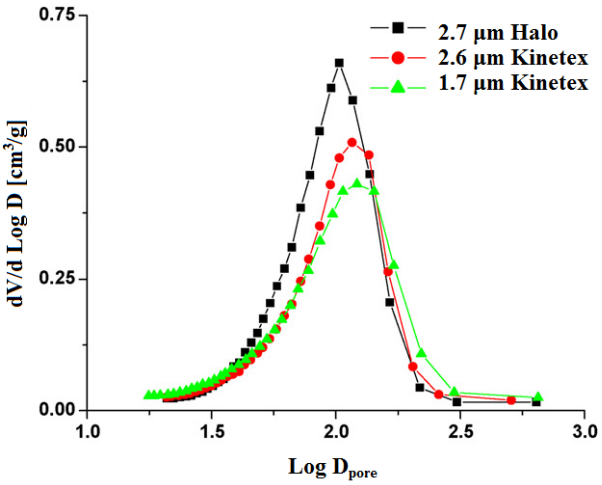

Fig. 2.5: Pore size distribution of three superficially porous particles (SPP) obtained from low temperature nitrogen adsorption data [39].

low temperature nitrogen adsorption (LTNA) at 77 K using the Brunauer-Emmett-Teller procedure (BET) or by mercury intrusion [14, 50, 51]. The former is based on the physisorption of gases while the latter is based on the controlled penetration of fluids. Both methods are based on certain assumptions, for example, on the pore shape. LTNA measurements are used for microporous and mesoporous silica but mercury intrusion is only good for mesoporous and macroporous silica. For mesoporous silica, nearly the same pore volume distributions were found by means of porosimetry and nitrogen sorption for mean pore diameters between 4 and 40 nm [14], however in other cases porosimetry gives slightly smaller values for the pore diameter [52]. Mercury intrusion does not work well for fragile particles (with a large pore volume and also for monolithic columns) or for soft polymer particles.

These techniques are either too expensive or they destroy the chromatographic column so it cannot be used for any further analysis. It is also possible that they give irrelevant information because fake assumptions are made while deriving values of parameters. For example it was long neglected that the size of nitrogen molecule is much smaller than the size of the analyte molecules used in chromatographic practice so that the pore volume derived from such measurements and the conclusions that were drawn could have been quite misleading [39].

The surface modification should also be taken into account. It was usually assumed, that the molecular area of nitrogen is 1.62 nm^2 [53] but it was

shown that nitrogen adsorption is less localized on hydrophobic surfaces due to weaker adsorbate-surface interactions and has more freedom for lateral movement, thus effectively occupying a larger area of the surface. Therefore the use of the 1.62 nm^2 value would lead to an underestimation of the actual surface area of hydrophobic surfaces and we should rather use 2.05 nm^2 [54].

Inverse Size Exclusion Chromatography (ISEC) is a very comfortable and preferred method to derive information about the structure of the porous packing material, such as the intersticial porosity of the packed bed or PSD of various porous particles and monoliths [6, 55–58]. ISEC has several advantages in comparison to other methods determining the porous structure. While in mercury intrusion and nitrogen absorption dry experimental environment with high pressure and low temperature are necessary that cause the structural damage of the porous material, in ISEC intact structural information of materials can be achieved without morphological changes. In addition, ISEC is operated under typical chromatographic conditions, so it is a relatively convenient approach [10]. It only needs an HPLC instrument with minor changes, is very gentle with the stationary phases and enables the determination of the PSD within the entire range of 1 to 400 nm of various types of stationary phases [59].

The porous structure of the chromatographic particles is of great complexity and that has a number of consequences during the separation process. The physico-chemical properties of HPLC stationary phases play an important role on column performance and efficiency. The proper characterization of the pore structure and the PSD is relevant, because the mass transfer across the particles is greatly affected by the nature of the pores.

Knox and Scott have developed a rather sophisticated model to determine the pore size distribution from SEC data [8]. The calibration curve of SEC can predict roughly the same PSD as mercury intrusion porosimetry results. The model has two assumptions: the pores should be cylindrical and the sample molecules should be spherical. For a continuous distribution of pore diameters they obtained the cumulative pore size distribution function ($G(R)$ where R stands for the pore cylinder's radius) by a simple differential procedure as

$$G(R) = K_{SEC} - \frac{3}{2}\left[\frac{dK_{SEC}}{d\ln r_G}\right] + \frac{1}{2}\left[\frac{d^2K_{SEC}}{d(\ln r_G)^2}\right], \tag{2.3}$$

where K_{SEC} is the partition coefficient in SEC, and r_G is the radius of the sample molecule.

2.3.3 Polydispersity

Size Exclusion Chromatography is more often used to obtain molecular size or molecular weight than for separating polymers from each other [60]. This determination relies on a calibration process where a number of special standard polymers with well-known molecular weight are eluted and a calibration curve is drawn by their partition coefficient ($\ln M_W$ vs. K). The retention properties of the unknown sample are then compared with the calibration data to determine the weight or size of the investigated molecule. Even though we say that these standards used for the calibration process have well-defined molecular weights, they do have a distribution. Manufacturers use a quantity to characterize the fitness-to-purpose of these polymers, the polydispersity (P).

The polydispersity of a polymer sample is defined as the ratio of the weight- and number-averaged relative molecular weights of the polymer sample [61]:

$$P = M_W / M_n \tag{2.4}$$

Although there is a new recommended IUPAC terminology for polydispersity [62] where 'degree-of-polymerization dispersity' and shortly the word 'dispersity' is recommended for use, we rather use the term polydispersity because this is still the common way how polymer scientist refer to the distribution of polymer molecules.

The knowledge and the effect of polydispersity – that it increases the peak width and leads to a decrease in separation efficiency – is almost of the same age as SEC [63–66]. It is very difficult, if feasible at all, to obtain experimentally the real polydispersity by SEC. However, the first equations that described the contribution of polydispersity to the height equivalent to a theoretical plate (HETP) value greatly underestimated the effect of polydispersity [63, 64], it was proven that similarly to a new equation given by Knox [61], the data given by the manufacturers overestimate it as well [67, 68].

As indicated in Eq. 2.1, the variances of the independent events can be divided into contributors and we can distinguish the contribution of the

kinetic events (σ^2_{kin}) and that of the polydispersity (σ^2_{P}) to the total band-broadening as

$$\sigma^2 = \sigma^2_{\text{kin}} + \sigma^2_{\text{P}}. \tag{2.5}$$

The elimination of the first term of Eq. 2.5 so the measurement of σ^2_{P} is experimentally impossible. Although recent improvements in experimental detection techniques in SEC made precise determination of molecular-weight-distribution possible, Netopilík showed that for samples with low polydispersity, the errors due to the band-broadening and due to the interdetector volume increases as polydispersity decreases [69]. The effect of polydispersity is in fact so large that even with $P = 1.01$ it is difficult to make accurate determinations of σ^2_{kin} because polydispersity of even a relatively narrow polymer fraction will contribute substantially to the total width of the eluted peak [61]. These results show that there is a need for a theoretical model to demonstrate the limitations of the contribution of polydispersity.

2.4 Size Exclusion Chromatography

Size Exclusion Chromatography is defined as the differential elution of solutes from the porous stationary phase caused by different degrees of steric exclusion [70]. The stationary phase used in SEC is always a mechanically stable porous media. The molecules traveling along the column in the mobile phase can enter the pores if the size of the pore is larger than that of the molecule. However it is still uncertain which exact size parameter determines the separation, in general it is accepted that the gyration radius or diameter of the molecule is used to determine whether the molecule can enter the pore [71].

In ideal SEC there is no interaction between the molecules and neither the stationary nor the mobile phase particles so that the separation is entropy-driven. There are however another mechanisms responsible for the migration of the molecules along the column (hydrodynamic and stress-induced diffusion, the polarization effect, multi-path, enthalpic and soft-body interactions and the so-called wall effect), they can be ignored in almost every case. The main mechanism responsible for retention of micromolecules in SEC is the size-exclusion effect [72] and for macromolecules it is the combination of the size-exclusion and the hydrodynamic effects [73].

There are two types of molecules that are of major importance in SEC based on their size: the completely permeable particle (indicated by a subscript 'perm' in the equations) that is small enough to visit all the pores, and the barely excluded particle that is too large to enter the pores and will be excluded (indicated by a subscript 'excl' in the equations). The former molecules have access to the stagnant and moving zone of the mobile phase as well while for the latter molecules only the interstitial volume between the stationary phase particles is available.

The operational aspects of SEC are presented in Fig. 2.6, where V_0 indicates the column void volume obtained by the retention volume of an excluded molecule, and V_{perm} is the volume available for the totally permeable molecules. Solutes of intermediate range have hydrodynamic radii between that of excluded and totally permeable molecules.

The partition coefficient (K_{SEC}) can easily be calculated by means of the retention volumes of the above mentioned and the unknown molecules by

$$K_{\mathrm{SEC}} = \frac{V_{\mathrm{i}} - V_{\mathrm{excl}}}{V_{\mathrm{perm}} - V_{\mathrm{excl}}} = \frac{V_{\mathrm{p}}}{V_{\mathrm{p,perm}}} = \frac{t_{\mathrm{p}}}{t_{\mathrm{p,perm}}}, \tag{2.6}$$

where after multiplication by the mobile phase velocity, the numerator stands for time spent by the investigated molecule in the pores of the stationary phase particles and the denominator indicates the residence time spent by the completely permeable particle in the pores (subscript p refers to pore).

As mentioned above, the retention of macromolecules arises from either size-exclusion effect, hydrodynamic effect or a combination of them according to their size relative to the pore size of the stationary phase [73]. Therefore, the retention volume (V_{R}) is written as

$$V_{\mathrm{R}} = V_{\mathrm{p}} K_{\mathrm{SEC}} + V_0 K_{\mathrm{HDC}} + V_{\mathrm{system}} \tag{2.7}$$

where K_{HDC} accounts for the hydrodynamic chromatography contribution and V_{system} is the volumetric contribution of the system [73, 74]. K_{HDC} is defined as

$$K_{\mathrm{HDC}} = \frac{1}{1 + 2\frac{r_{\mathrm{eff}}}{r_0} - C\left(\frac{r_{\mathrm{eff}}}{r_0}\right)^2} \tag{2.8}$$

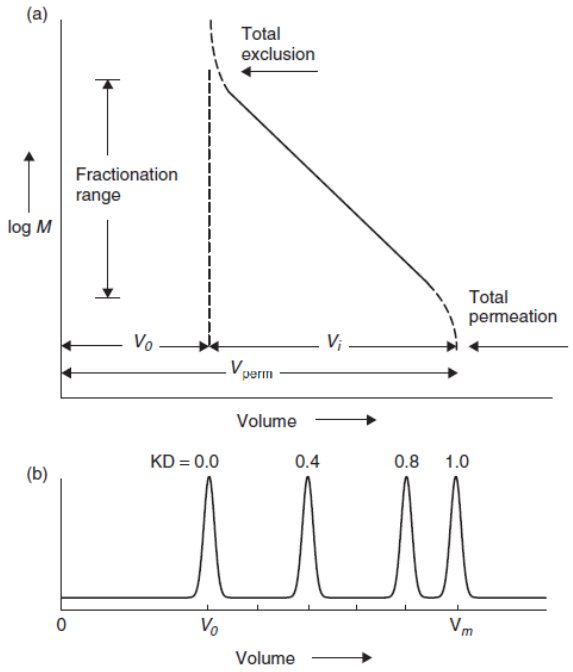

Fig. 2.6: Hypothetical SEC calibration curve (a) and chromatogram (b) [1]

where C is a constant which depends on the packing-carrier-polymer system (here $C = 2.698$ [75]), r_0 the hydraulic radius of the packing material and r_{eff} the effective size of macromolecule:

$$r_{\text{eff}} = \frac{\sqrt{\pi}}{2} r_{\text{G}} \tag{2.9}$$

where r_{G} is the mean gyration radius of the molecule. It was shown [74] that by combining the Kirkwood–Riseman relationship with the Stokes–Einstein equation, one gets a direct relation of the gyration radius to the molecular weight (M_{W}) as

$$r_{\text{G}} = \frac{k_{\text{B}} T M_{\text{W}}^{B}}{4\pi\eta K}, \tag{2.10}$$

where k_{B} is the Boltzmann constant, T is the temperature, η is the viscosity of the mobile phase, B is the exponent of the power law relating the diffusion coefficient of the polymer to the reciprocal of its molecular weight and K is a constant. Since K and B are tabulated for various polymer–solvent systems, r_{G} can safely be used. The typical value for B is 0.549 and for K is 3×10^{-8} m^2/s [74]. The hydraulic radius of the packing material, r_0 is:

$$r_0 = \frac{d_{\text{p}}}{3} \frac{\varepsilon_{\text{e}}}{1 - \varepsilon_{\text{e}}} \tag{2.11}$$

where d_p is the diameter of the particle and ε_e is the external porosity of the packing material.

In a widely used retention model [60, 74, 76] the ratio of the gyration radius of the molecule (r_G) to the radius of the pore opening (r_p) is a unique size parameter:

$$\rho = \frac{r_G}{r_p}, \tag{2.12}$$

which is used to define the partition coefficient as

$$K_{SEC} = \begin{cases} (1-\rho)^m & \text{if } 0 \le \rho \le 1 \\ 0 & \text{if } \rho > 1 \end{cases} \tag{2.13}$$

where m is a constant whose value depends only on the pore geometry.

SEC can be used to determine the molecular weight or size of a molecule by a calibration process (see Section 2.3.3), and by using the inverse way, ISEC is an appropriate tool to investigate the properties of the stationary phase (pore geometry and PSD). For the effective use of ISEC however a proper theory is needed which relates PSD to the retention time of polymers. The stochastic theory seems rather suitable for describing SEC among the basic theories of chromatography.

2.5 Stochastic theory of Size Exclusion Chromatography

The molecular, or stochastic theory of chromatography is a microscopic model introduced by Giddings and Eyring in 1955 for adsorption chromatography [77]. It uses random variables and probabilistic terms to describe the migration of the molecules along the chromatographic column at a molecular level. The theory assumes that, if we ignore the axial dispersion, the number of adsorption and desorption steps is determined by a Poisson process and the time that a molecule spends bound to the stationary phase (residence or sojourn time) is determined by an exponential distribution. The stochastic theory is completely independent of the physical-chemical mechanisms responsible for the retention; therefore it can be used in any field of chromatography. Accordingly, the model has been extended and improved for several chromatographic methods such as adsorption, partition,

ion-exchange or Size Exclusion Chromatography. It was adapted to SEC by Carmichael [78–81].

The stochastic approaches may become very complex to work with for situations except the most simple case of adsorption, so it was not conveniently used until the characteristic function (CF) approach was introduced to this field [82]. The CF method made the use of stochastic theory of chromatography simpler even for complicated cases such as heterogeneous adsorption chromatography [83]. Later the effects of the mobile phase dispersion were introduced (stochastic-dispersive model) and they involved an increasing number of parameters specified in the description of the system [84].

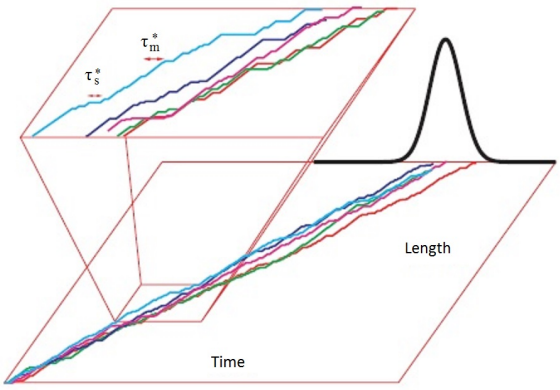

Fig. 2.7: Chromatography as a stochastic process. The elution profile is the probability density function of the retention times of the individual molecules.[85]

SEC is based on the random migration of molecules, where randomly occurring entrapment and release of molecules in the mesopores of the stationary phase builds up the separation process. The stochastic theory of SEC assumes that a molecule of a certain size enters and leaves the pores n_p times on average during the migration along the column and spends τ_p time on average in a single pore. After leaving a pore, the molecule spends τ_m time on average in the mobile phase before entering another pore. All these variables are random quantities, therefore each molecule has an individual path while migrating along the column (Fig. 2.7). However the molecules of the same size behave in a similar manner, because of the anomalies in the retention paths of the molecules we observe a nearly Gaussian curve as chromatographic peak. The observed retention time of a peak is the mean of the distribution of the individual retention times and the width of the peak is described by the standard deviation.

The average number of the pore ingress steps (if ρ takes a value between 0 and 1) can be written as

$$n_{\mathrm{p}} = n_{\mathrm{perm}} (1 - \rho)^{m_{\mathrm{e}}}, \tag{2.14}$$

and the residence time in the pores will be:

$$\tau_{\mathrm{p}} = \tau_{\mathrm{perm}} (1 - \rho)^{m_{\mathrm{p}}}, \tag{2.15}$$

residence time spent by the completely permeable particle

where n_{perm} and τ_{perm} are the average number of the pore ingress steps and the average time spent in a single pore by a completely permeable particle, respectively, and m_{e} and m_{p} are constants depending on the ingress and the egress processes, respectively. Both of n_{p} and τ_{p} take the value 0 if $\rho > 1$.

As Dondi et al. showed earlier [76], parameters m_e, m_{p} and m are related as

$$m = m_{\mathrm{e}} + m_{\mathrm{p}}, \tag{2.16}$$

where the geometry parameter, m is exactly the same as in Eq. 2.13. Thus it can be seen that both the pore ingress and egress processes affect the selectivity of SEC.

The relationship between m, m_{e}, and m_{p} can be re-expressed when we introduce parameter α to characterize the relative contribution of the pore egress process to the overall size-exclusion effect [86]:

$$\alpha = \frac{m_{\mathrm{p}}}{m}. \tag{2.17}$$

The characteristic function is the main equation of the stochastic theory. Formally it is the Fourier transform of the elution profile and it contains all the information about the separation process. In this simple case the following CF describes the system the best:

$$\phi(\omega) = \exp\left\{ n_{\mathrm{p}} \left[\frac{1}{1 - i\omega\tau_{\mathrm{p}}} - 1 \right] \right\}, \tag{2.18}$$

where i is the imaginary unit and ω is an auxiliary real variable (frequency). In this case the probability density function (PDF) (the time-domain signal) can be written as the inverse Fourier transform of the CF as:

$$f(t) = \sqrt{\frac{n_\mathrm{p}}{t\tau_\mathrm{p}}} e^{-t/\tau_\mathrm{p} - n_\mathrm{p}} I_1\left(\sqrt{\frac{4n_\mathrm{p}t}{\tau_\mathrm{p}}}\right), \tag{2.19}$$

where I_1 is a modified Bessel function of the first kind and first order.

There is a simple relationship between the CF and the moments about the origin. The kth moment of the chromatographic peak can be calculated from the CF (Eq. 2.18) by the moment theorem of the Fourier transform as

$$\mu_k = i^{-k}\left[\frac{\mathrm{d}^\mathrm{k}\phi(\omega)}{\mathrm{d}\omega^\mathrm{k}}\right]_{\omega=0}. \tag{2.20}$$

It is well-known that the first moment is the mean residence time and the second central moment is the variance of the observed chromatographic peak. The third central moment gives information about the peak symmetry. Using the equation above we obtain these moments as

$$\mu_1 = n_\mathrm{p}\tau_\mathrm{p}, \tag{2.21}$$

$$\mu_2' = 2n_\mathrm{p}\tau_\mathrm{p}^2, \tag{2.22}$$

$$\mu_3' = 6n_\mathrm{p}\tau_\mathrm{p}^3. \tag{2.23}$$

The above equations are only valid if we assume that the pore size in the stationary phase particles is uniform.

For heterogeneous kinetics, the simplest stochastic model cannot be employed. Cavazzini et al. extended the stochastic model of chromatography to the case where the stationary phase consists of more than one types of adsorption sites and for the case when the adsorption energy of the sites is determined by a distribution [83]. It was assumed that if there are several types of adsorption sites in the column, the molecules bind with a certain probability to each of them. Thus, the PDF describing the peak shape can be obtained as the probability-weighted convolution of the PDFs of the different

sites. For example, for two different adsorption sites the following CF was obtained:

$$\phi(\omega) = \exp\left\{n_1\left[\frac{1}{1-i\omega\tau_1}-1\right]\right\}\exp\left\{n_2\left[\frac{1}{1-i\omega\tau_2}-1\right]\right\} \tag{2.24}$$

The corresponding peak shape is:

$$\begin{aligned} f(t) = &\left(\sqrt{\frac{n_1}{t\tau_1}}e^{-t/\tau_1-n_1}I_1\left(\sqrt{\frac{4n_1t}{\tau_1}}\right)\right) \\ &* \left(\sqrt{\frac{n_2}{t\tau_2}}e^{-t/\tau_2-n_2}I_1\left(\sqrt{\frac{4n_2t}{\tau_2}}\right)\right), \end{aligned} \tag{2.25}$$

where the subscripts refer to the respective sites and the sign $*$ stands for convolution. The calculation of the moments and that of the peak profile is difficult in time domain – if it is possible at all, so it cannot practically be used in this form.

3 Experimental and methods

> *It doesn't matter how beautiful your theory is, it doesn't matter how smart you are. If it doesn't agree with experiment, it's wrong.*
>
> — **Richard P. Feynman**

3.1 Calculations

To derive the models for stochastic theories containing the effects of pore size distribution and polydispersity, all calculations were carried out with the software package Mathematica 9 (Wolfram Research). The elution profiles were obtained via numerical inverse Fourier transform using 1024 points. In all cases $r_{p,0}$ was set to 12.434 nm based on the value obtained for the Aeris Widepore stationary phase. The other parameters used for a certain calculation are indicated there. The moments were obtained using the equations derived below and validated via integration of the peak profiles.

Monte Carlo simulation by generating one million normally distributed random numbers was carried out in Mathematica 9 to show the relationship between the breadth of the molecule size distribution and the polydispersity.

Iterative alignments were performed in Gnuplot using the data obtained from the ISEC measurements.

3.2 Tools and materials

The measurements were carried out at the Department of Analytical and Environmental Chemistry, University of Pécs. An Agilent 1100 liquid chromatograph equipped with a dual solvent delivery system, an auto sampler, a

column thermostat and a diode array UV detector was used for all measurements. Data were collected with Chemstation software. The following C_{18} columns were used (data given by manufacturers):

- Columns packed with superficially porous particles (SPP):
  - Phenomenex Aeris Peptide (d_p=3.6 µm, d_{core}=2.6 µm, r_p=5 nm),
  - Phenomenex Aeris Widepore (d_p=3.6 µm, d_{core}=3.2 µm, r_p=10 nm),
  - Phenomenex Kinetex (d_p=2.6 µm, d_{core}=1.9 µm, r_p=5 nm),
  - Phenomenex Kinetex (d_p=5 µm, d_{core}=3.6 µm, r_p=5 nm),
- Columns packed with totally porous particles (TPP):
  - Zorbax Eclipse Plus (d_p=3.5 µm, r_p=4.75 nm),
  - Waters Symmetry (75×4.6 mm, d_p=3.5 µm, r_p=5 nm),
  - Waters Symmetry (150×4.6 mm, d_p=5 µm, r_p=5 nm),
- Monolithic columns:
  - Chromolith Performance (fully end-capped),
  - Chromolith HighResolution (fully end-capped),

where d_p and d_{core} are the total diameter and the core diameter of the stationary phase particle, respectively. Each column (other than the Waters Symmetry ones) was of 100×4.6 mm. The Phenomenex Kinetex columns and the Waters Symmetry columns will be distinguished by their particle diameters, so that Kinetex 2.6 µm, Kinetex 5 µm, Symmetry 3.5 µm and Symmetry 5 µm will be listed. The Phenomenex Aeris Peptide, Phenomenex Aeris Widepore and Zorbax Eclipse Plus columns will be referred to as Aeris Peptide, Aeris Widepore and Zorbax, respectively. The Chromolith Performance column will be referred to as first generation monolith while the Chromolith HighResolution column as second generation monolith.

For the success of the ISEC procedure, one should use standards with low polydispersity and a mobile phase strong enough to eliminate solute interaction with the stationary phase. Polystyrene standard were purchased from Varian, (Varian, Inc. USA). The molecular weights (M_W), polydispersities (P) and the calculated gyration radii (r_G) of them are listed in Table 3.1.

HPLC grade tetrahydrofuran (THF), purchased from Fisher Scientific (Fisher Scientific, Ltd. UK) was used at all experiments. The viscosity of THF was 0.55 mPa s (293.15 K). The mobile phase flow rate was kept at 0.50 cm^3/min for eluting the single polystyrene standards. Each measurement was executed with 100% THF containing eluent. The column thermostat was set at 293.15 K.

Tab. 3.1: Polystyrene standards used for obtaining experimental data; polydispersity data are given by manufacturer, r_G was calculated using Eq. 2.10.

M_W (Da)	P	r_G (nm)
580	1.12	0.736
1480	1.06	1.231
1530	1.07	1.253
3070	1.04	1.837
3950	1.03	2.109
6930	1.03	2.872
10,110	1.02	3.532
31,420	1.02	6.585
70,950	1.03	10.299
170,800	1.02	16.682
578,500	1.02	32.593
1,233,000	1.05	49.381
1,412,000	1.04	53.196
2,782,100	1.04	77.193
3,250,000	1.04	84.070

The concentration of all the samples was 0.50 mg/cm^3 dissolved in THF. The injected volume was 1.00 µL. The components were detected at 254 nm. The retention volumes of polystyrene standards were corrected for the extra-column volume measured at the same condition for each polymer.

The average extra-column volume (V_{system}) was $0.050 \pm 5.698 \times 10^{-4}$ cm^3 for the packed beds and $0.070 \pm 7.98 \times 10^{-4}$ cm^3 for the monoliths. This difference was observed because a capillary tube was exchanged by service between the consecutive experiments.

4 Results and discussion

> *As far as the laws of mathematics refer to reality, they are not certain; and as far as they are certain, they do not refer to reality.*
>
> — **Albert Einstein**

4.1 Effect of pore size distribution

In Size Exclusion Chromatography (SEC), the most important factor is the pore size of the stationary phase, since the separation is based on the size of the analyte molecules relative to the pore size.

In ideal SEC, because there is no physico-chemical interaction between the sample molecules and the stationary phase surface, the type of the silica and the chemical modification have no effect on the retention and on the selectivity. The size of the stationary phase particles of the modern HPLC columns varies in a quite wide range, and it has been recently demonstrated that there is no evident correlation between the particle size distribution and column efficiency [47]. The effect of the structure of the stationary phase particle (e.g. non-porous particles, TPP, SPP) on the separation efficiency is quite significant, because diffusion within the particles has a strong impact on the brand broadening in all modes of HPLC. The size-exclusion effect does not exist on non-porous particles, only the hydrodynamic effect is present. The totally porous particles have a large pore volume where the molecules can diffuse and macromolecules may spend long time there, thus slow pore diffusion gives rise to band broadening of the observed peaks. In the case of the superficially porous particles the pore volume is more limited and the diffusion times are shorter [87].

Results obtained with LTNA confirmed that the presently commercially available HPLC columns do not have a uniform pore size, but contain pores in a relatively wide pore size range [39]. This is an important aspect, because molecules of a given size are not equally likely to enter each pore which ultimately leads to the distortion in the peak shapes in practice.

4.1.1 Model derivation – Integrating pore size distribution into the stochastic theory of Size Exclusion Chromatography

The stochastic theory describes the chromatographic process at the molecular level so it is obvious to introduce the pore size distribution (PSD) into that in order to obtain more relevant information about the retention properties. The concept introduced by Eq. 2.24 can be extended to multisite heterogeneous adsorption and the following characteristic function is obtained when x type of sites are present, each with a relative abundance of p_j, $(j = 1, \ldots, x)$ [83]:

Sepsey, A., Bacskay, I., Felinger, A., Molecular theory of Size Exclusion Chromatography for wide pore size distributions, J. Chromatogr. A, 2014, 1331, 52–60.

$$\phi(\omega) = \exp\left\{ n \left[\sum_{j=1}^{x} p_j \frac{1}{1 - i\omega\tau_j} - 1 \right] \right\}. \tag{4.1}$$

Equation 4.1 can be extended for a continuous distribution of sites.

When modeling SEC, one can use the same idea. The only thing we should change is the nomenclature used, so that we say pore entrance and release instead of adsorption and desorption, respectively.

If all the pores were of the same size, one would obtain the characteristic function and the moments of the band profile as written by Eqs. 2.18 to 2.20. However, when the pore size is governed by a distribution, the PDF of the PSD ($\zeta(r_p, r_{p,0}, \sigma)$) must be included and we should replace r_p by that PDF in Eq. 2.12 and thus in Eqs. 2.14 and 2.15, because both the number of pore entries and the individual sojourn times of the molecules in a pore depend on the size of the molecule relative to the size of the pore. Then the characteristic function could be obtained by combining the PDF of the PSD with the characteristic function as

$$\phi(\omega, r_p) = \exp\left[\int_{r_G}^{\infty} \zeta(r_p, r_{p,0}, \sigma) n_p \left(\frac{1}{1 - i\omega\tau_p} - 1 \right) \mathrm{d}r_p \right]. \tag{4.2}$$

Experimental evidence shows that the PSD of HPLC packing materials can be described by a log-normal distribution [39]. Thus the PDF used for $\zeta(r_\mathrm{p}, r_{\mathrm{p},0}, \sigma)$ is

$$\zeta(r_\mathrm{p}, r_{\mathrm{p},0}, \sigma) = \frac{1}{\sqrt{2\pi}\sigma r_\mathrm{p}} \exp\left(-\frac{(\ln r_\mathrm{p} - \ln r_{\mathrm{p},0})^2}{2\sigma^2}\right), \tag{4.3}$$

where $r_{\mathrm{p},0}$ and σ represents the maximum and width of the log-normal distribution, respectively. One should note that the true first absolute and second central moments of the log-normal distribution (Eq. 4.3) are

$$\mu_{1,\mathrm{log-norm}} = r_{\mathrm{p},0} e^{\sigma^2/2}, \tag{4.4}$$

and

$$\mu'_{2,\mathrm{log-norm}} = r_{\mathrm{p},0}^2 e^{\sigma^2}\left(e^{\sigma^2} - 1\right). \tag{4.5}$$

For the sake of simplicity, however, further on we refer to $r_{\mathrm{p},0}$ and σ as the mean and the standard deviation of the log-normal distribution, respectively.

We obtain the characteristic function in the case of log-normal PSD when we combine Eqs. 4.2 and 4.3 as

$$\phi(\omega) = \exp\left[\frac{1}{\sqrt{2\pi}\sigma}\int_{r_\mathrm{G}}^{\infty} \frac{n_\mathrm{p}(r_\mathrm{p})}{r_\mathrm{p}} \exp\left(-\frac{(\ln r_\mathrm{p} - \ln r_{\mathrm{p},0})^2}{2\sigma^2}\right) \cdot \right.$$
$$\left. \cdot \left(\frac{1}{1 - i\omega\tau_\mathrm{p}(r_\mathrm{p})} - 1\right) \mathrm{d}r_\mathrm{p}\right]. \tag{4.6}$$

The above characteristic function describes the peak shape in Fourier domain for SEC when the pore sizes are not uniform. The peak shape itself can be calculated as the inverse Fourier transform of $\phi(\omega)$. Unfortunately, Eq. 4.6 cannot be evaluated analytically for the general case. Nevertheless, the calculation of the moments is possible in some cases. An analytical expression of the moments can only be obtained if parameters m_e and m_p are both integers. Intuition suggests and extensive data processing of SEC data confirms that for the ingress process $m_\mathrm{e} > 0$ in Eq. 2.14 and for the egress process $m_\mathrm{p} < 0$ in Eq. 2.15 [86].

The first absolute moment as well as the second and the third central moments of the elution profile will be obtained respectively from Eq. 4.6 using Eq. 2.20 as

$$\mu_1 = n_{\text{perm}} \tau_{\text{perm}} a, \tag{4.7}$$

$$\mu_2' = 2 n_{\text{perm}} \tau_{\text{perm}}^2 a, \tag{4.8}$$

$$\mu_3' = 6 n_{\text{perm}} \tau_{\text{perm}}^3 a. \tag{4.9}$$

By substituting Eq. 2.14 and Eq. 2.15 into Eq. 2.21 and using 2.13 we compare the obtained expression with Eq. 4.7, we can see that parameter a is actually equal to K_{SEC} and has the form of

$$a = K_{\text{SEC}} = \frac{1}{2} \sum_{k=0}^{\varphi} (-\rho)^k e^{\frac{k^2\sigma^2}{2}} \binom{\varphi}{k} \operatorname{erfc}\left(\frac{k\sigma^2 + \ln \rho}{\sqrt{2}\sigma} \right). \tag{4.10}$$

Parameter a – and thus K_{SEC} – strongly depends on the pore shape. To obtain the first absolute moment, μ_1, $\varphi = m_{\text{e}} + m_{\text{p}}$ should be used which is equal to m thus depending on $\varphi = 1$, 2 or even 3, the pore is slit shaped, cylindrical or conicalspherical, respectively. The second central moment can be calculated using $\varphi = m_{\text{e}} + 2m_{\text{p}}$, and the third central moment by using $\varphi = m_{\text{e}} + 3m_{\text{p}}$.

The correctness of the derived moments can be justified by calculating their limit values in $\sigma \to 0$. These limits give in all cases Eqs. 2.21–2.23 where Eqs. 2.14–2.15 are used.

Parameter a can only be calculated by Eq. 4.10 when $\varphi > 0$. For instance, when $m = 3$ and $\alpha = -1$, thus $m_{\text{p}} = -3$ and $m_{\text{e}} = 6$, while calculating the third central moment, φ would be -3 and the analytical calculation of that moment is not possible with the equations written above. Nevertheless, the first and the second moments can be still evaluated. The first three moments can be calculated in all the cases when $\alpha \geq -0.5$. For $\alpha < -0.5$ one would get $\varphi < 0$ for the calculation of the third moment and it is not possible to use Eq. 4.10 in 4.9.

One can always obtain the elution profile with the inverse Fourier transform of Eq. 4.6 and calculate the moments by numerical integration of the peak profile.

4.1.2 Graphical demonstration of the novel model

The equations above demonstrate that PSD will have important consequences on retention time and peak shape. We obtain the relative pore accessibility by plotting parameter a against the size ratio, ρ when no pore geometry is assumed, i.e. $m = 0$ and a certain value of the standard deviation of the PSD is substituted. This is illustrated in Fig. 4.1/a). In the case of uniform pores ($\sigma = 0$), there is a sharp distinction between the molecules that visit the pores and the ones that are excluded. All the molecules that are small enough to fulfill $\rho < 1$, i.e. molecules for which $r_G < r_p$ can visit all the pores. On the other hand, every molecule for which $\rho > 1$ is excluded from all the pores. However, when a range of pore sizes are present in the stationary phase so that $\sigma > 0$, there are pores that are accessible for the molecules larger than $r_{p,0}$ too. The broader the PSD, the smoother is the transition between inclusion and exclusion. The rest of Fig. 4.1 shows the effect of ρ and σ on the partition coefficient in case of $m = 1$ (slit shaped pore geometry), $m = 2$ (cylindrical pore geometry) and $m = 3$ (conical or spherical pore geometry), respectively.

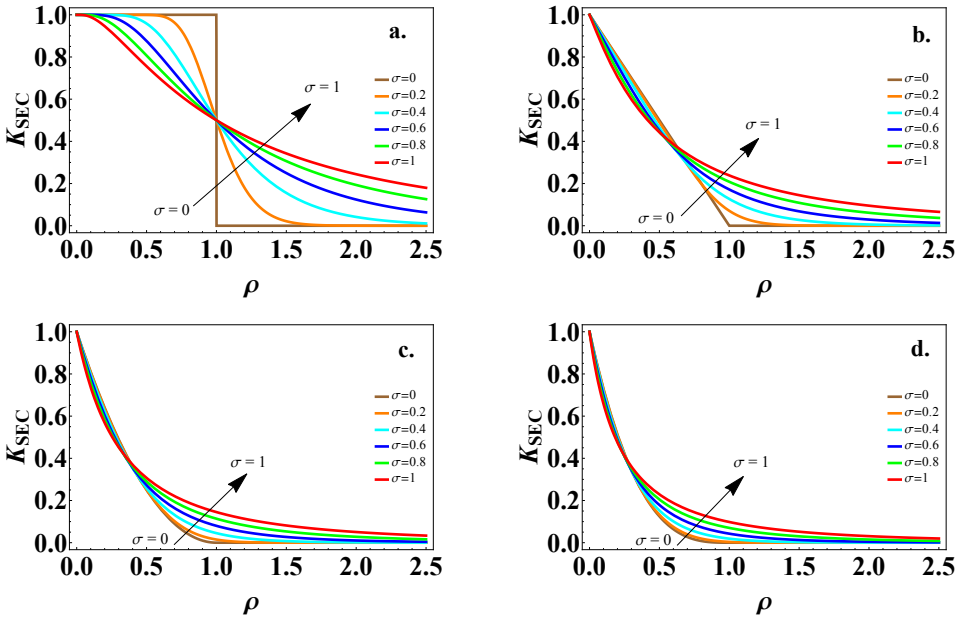

Fig. 4.1: The influence of the pore shape parameter (m) and the size of the molecule relative to the pore size (ρ) on the partition coefficient when a; the pore geometry is not included ($m = 0$, relative pore accessibility), b; slit shaped pores ($m = 1$), c; cylindrical pores ($m = 2$) and d; conical or spherical pores ($m = 3$).

To exploit the effect of the PSD on the elution profile, we calculated various chromatograms by changing the standard deviation of the PSD and the size of the solute molecule relative to the pore size. As mentioned in the experimental section (Section 3.1), the mean pore size ($r_{p,0}$) was set to 12.434 nm in the calculations to demonstrate the effect of the PSD. The PDFs of the log-normal distribution used for demonstrations are shown in Fig. 4.2.

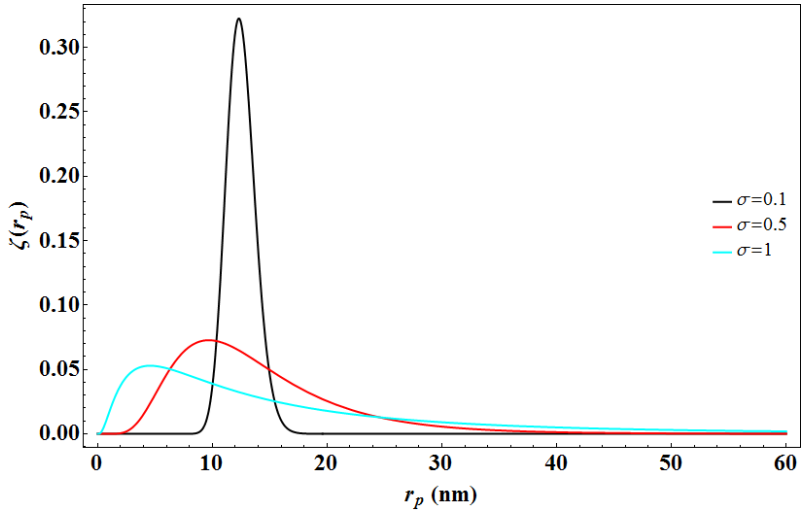

Fig. 4.2: Probability density functions of the log-normal distribution when the mean of the pore size is $r_{p,0} = 12.434$ nm and the breadth of the distribution (σ) is 0.1, 0.5 and 1, respectively.

The effect of increasing the breadth of the PSD (σ) on the chromatograms can be seen in Fig. 4.3 for a relatively large molecule, when the relative size parameter is $\rho = 0.95$. This figure illustrates the positive effect of the PSD on the chromatographic process, where the solid lines represent $\sigma = 0.1$, the long-dashed lines amounts to $\sigma = 0.5$ and the short-dashed lines stand for $\sigma = 1$. Depending on the pore shape, the retention times of the profiles vary in a quite wide range. However, it can be seen in all cases that the retention time increases and the skew of the elution profile decreases as σ increases. The assumed sample molecules are very large, they rarely can get inside the pores. Once they enter a pore however, they cannot escape from it and the molecule remains trapped at the same position as time passes (n is very small and τ is very large). Most of the molecules, however, cannot enter a pore and for this reason they are unretained and elute at the void time. This is best illustrated by the green solid line that stands for conical or spherical pore shape ($m = 3$) and relatively small standard deviation ($\sigma = 0.1$) in Fig. 4.3. This narrow distribution is also demonstrated for the case of cylindrical pores, where we obtain an exponential decreasing line as

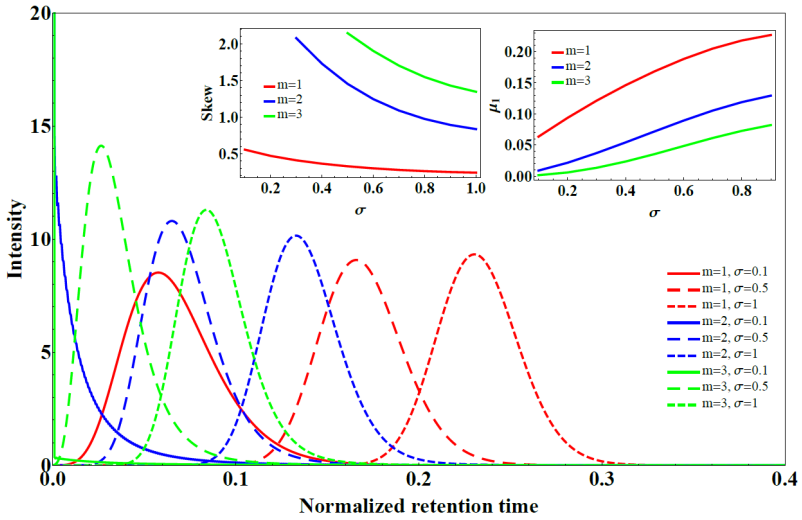

Fig. 4.3: The effect of the breadth of the PSD (σ) on the calculated chromatograms for slit shaped pores, for various pore geometries when the size parameter ρ is 0.95. In the inserts the changes in the skew and in the first absolute moment of the chromatograms are plotted.

the elution profile. As the standard deviation of the pore size is increased, the elution profile becomes a Gaussian peak and if $\sigma = 1$ one obtains the most symmetric profile for every kind of pore shape.

For smaller molecules ($\rho = 0.1$ to 0.5), the trends when σ is increased are rather different depending on the pore shapes. In case of slit shaped pores, σ has a more dominant effect on the K_{SEC} value than for the other pore geometries. This was already demonstrated in Fig. 4.1. For example if the particular molecular size equals to the half of the average pore size i.e. $\rho = 0.5$, the retention time would increase when $m = 2$ or 3 and decrease when $m = 1$ while increasing σ. Simultaneously the chromatograms become more asymmetrical which is most significant for conical pore geometry ($m = 3$). For smaller ρ values the retention time will decrease for each pore geometry while σ is increased.

The relative molecule size (ρ) is of utmost effect on the retention time, i.e. on the first moment. The larger the ρ, the less the molecule is included. By calculating the skew of the peak profiles, we can see that the peaks become more asymmetrical as ρ increases. Chromatograms are plotted in Fig. 4.4 for different pore shapes and molecular sizes. The retention times of the observed chromatogram changes considerably. We can conclude that the PSD has only slight influence on the behavior of the small molecules while its effect on the large molecules ($\rho > 0.5$) is intensive. The larger the molecule,

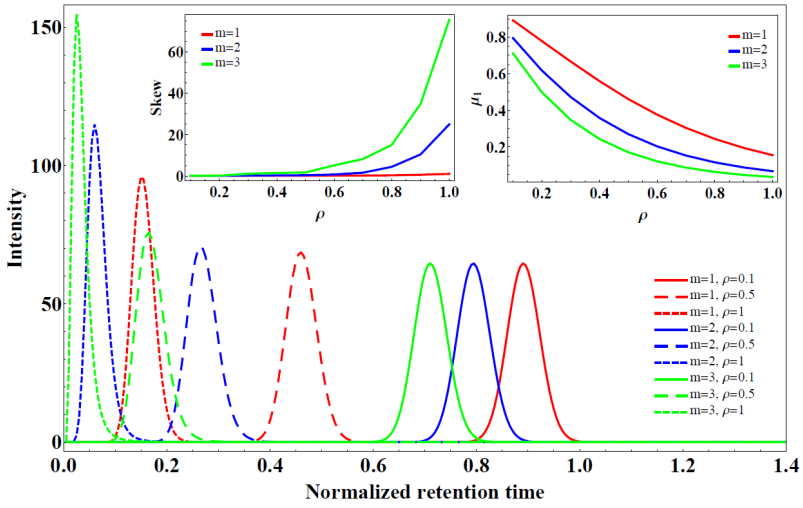

Fig. 4.4: The effect of the size parameter (ρ) on the calculated chromatograms for slit shaped pores, for cylindrical pores and for spherical or conical pores when the breadth of the PSD is $\sigma = 0.5$. In the inserts the skew and the first absolute moment of the chromatograms are plotted.

the harder it can enter the pores, but once it enters a pore it gets stuck there and remains at the same position as time passes. That is why the peaks of large molecules slightly below the exclusion limit (i.e. with high ρ values) become extremely broad and skewed.

Parameter α expresses the relation of the pore ingress and egress processes (see Eq. 2.17). We calculated elution profiles for various α values for the three mentioned pore shapes. The observed profiles are demonstrated in Fig. 4.5 where the relative size parameter (ρ) was set to 0.95 and the variance of the PSD was $\sigma = 0.5$. In this configuration the size of the sample molecules is very close to the pore size, however the effects of changing the parameter α is very meaningful. As it could be expected, the retention time (the first moment) does not depend on α. The second central moment and the skew of the observed profiles increase as α decreases. This is demonstrated in the subfigures of Fig. 4.5. Assuming slit shaped pores ($m = 1$), the relation of the ingress and egress processes does not affect the peak symmetry as much as in the other geometries ($m = 2$ and 3) where the peaks become more asymmetrical as α increases. The same tendency could be observed for all values of ρ: the profiles become more asymmetrical as α decreases.

From the results presented in Figures 4.3 to 4.5 we can conclude that the effect of the parameters studied (ρ, σ, α) is the most intensive in case of

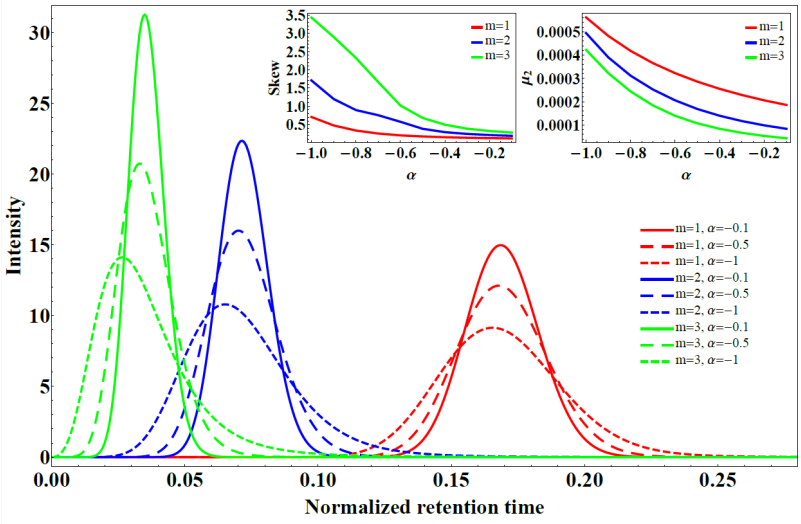

Fig. 4.5: The effect of the relative contribution of the pore egress process to the overall size-exclusion effect (α) on the calculated chromatograms for slit shaped pores, for cylindrical pores and for spherical or conical pores when the size parameter is $\rho = 0.95$, and the breadth of the PSD is $\sigma = 0.5$. In the inserts the changes in the skew and in the second central moment of the chromatograms with α are plotted.

conical or spherical pores and the least intensive when slit shaped pores are assumed.

We investigated how the peak resolution and the efficiency of the separation are affected by the PSD. The analytical calculation of the relative resolution is only possible if the first absolute and the second central moments of the peak are calculated for integer m_e and m_p values. There are only a few situations this calculation can be done.

The change of the resolution and the number of theoretical plates with the breadth of PSD are reported in Figures 4.6 and 4.7. Several important conclusions can be drawn from the data presented in the figures. Based on the molecule size, the curves can be divided into two cases. In the first case, the molecules are small enough to separate them by SEC and neither the relative resolution nor the number of theoretical plates is affected by the PSD. This can be seen in Figs. 4.6 and 4.7, where the plots referring to the small molecules (small ρ values) hardly show any change as σ increases, while the relative resolution and the number of theoretical plates for the larger and especially for the largest molecules (higher ρ values) significantly increase as σ increases. The effect is stronger as the value of m increases

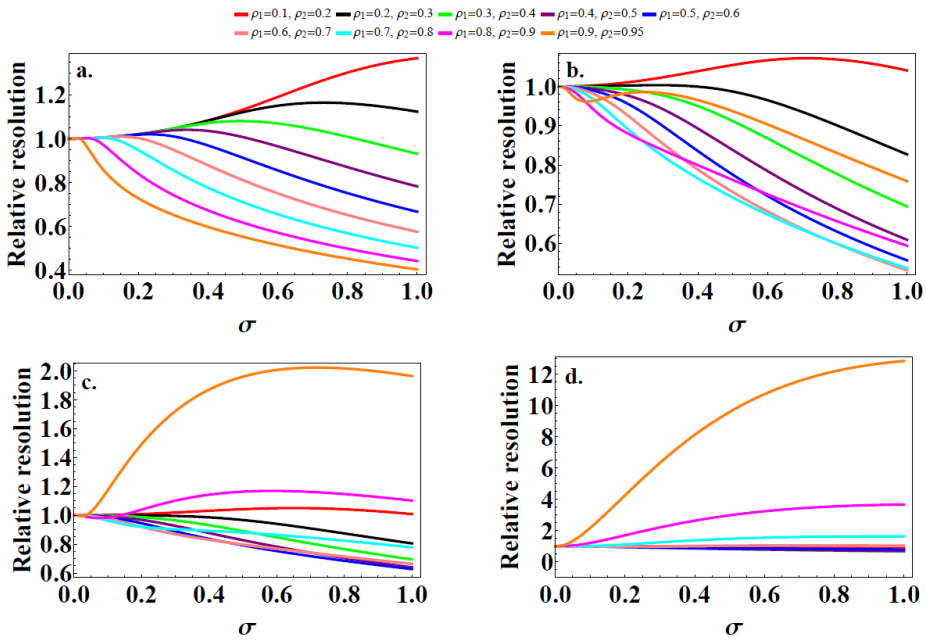

Fig. 4.6: Relative resolution for calculated chromatograms of differing size parameters (ρ). The pore shape parameter (m) and the relative contribution of the pore egress process to the overall size-exclusion effect (α) were varied as a; $m = 1$ and $\alpha = -1$, b; $m = 2$ and $\alpha = -0.5$, c; $m = 2$ and $\alpha = -1$ and d; $m = 3$ and $\alpha = -1$.

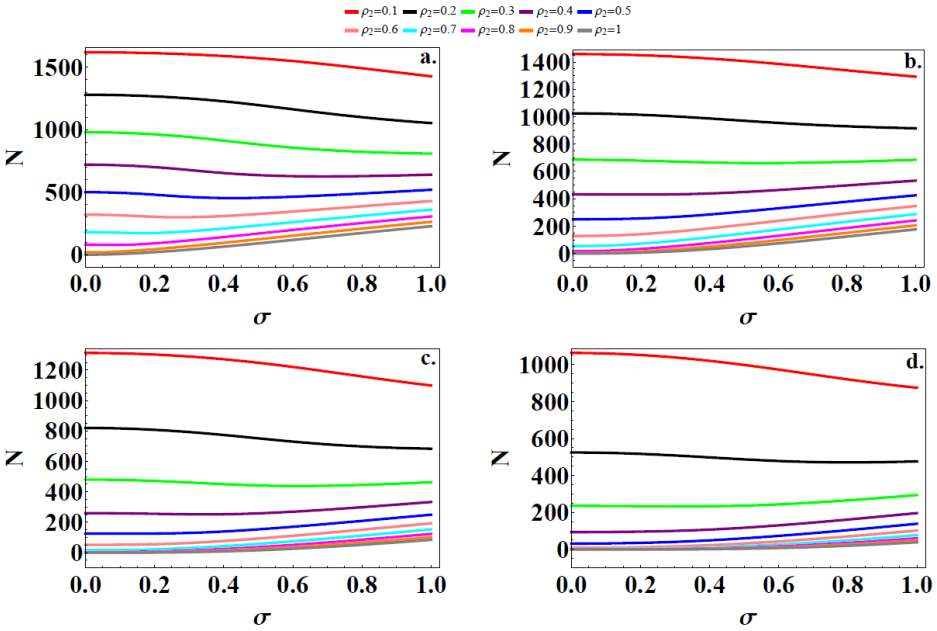

Fig. 4.7: Number of theoretical plates for calculated chromatograms of differing size parameters (ρ). The pore shape parameter (m) and the relative contribution of the pore egress process to the overall size-exclusion effect (α) were varied as a; $m = 1$ and $\alpha = -1$, b; $m = 2$ and $\alpha = -0.5$, c; $m = 2$ and $\alpha = -1$ and d; $m = 3$ and $\alpha = -1$.

(i.e. in the case of cylindrical and spherical or conical pores relative to slit shaped pores).

This observation drives us to more general conclusions in the field of chromatography, because the size-exclusion effect is not only important in SEC, but also in other chromatographic methods, such as reversed phase or Hydrophilic interaction chromatography (HILIC) separations of macromolecules. In those cases, the hindered pore diffusion is very important, and the size-exclusion process becomes more important than the other effects of the retention.

4.2 Pore structure determination of various columns

Based on the model derived in Section 4.1, we determined the pore structure (porosity, PSD and geometry) of nine commercially available C_{18} columns. Three of them were packed with totally porous particles, four of them were packed with superficially porous particles and two of them were monoliths of 1G and 2G, respectively. All measurements were executed at the same conditions, i.e. on the same instrument, with neat THF eluent, at the same temperature and flow rate, using polystyrene standards as indicated in the experimental part (Section 3.2). First, the results obtained for TPP and SPP filled columns are represented. In the second part of this section, the two generations of monolith columns are compared based on their structural properties.

4.2.1 Pore size distribution and pore geometry of superficially porous and totally porous particles

The polystyrene standards listed in Table 3.1 were injected individually on each column. Fig. 4.8 shows a series of superposed size-exclusion chromatograms obtained on a Phenomenex Aeris Widepore column. According to the size-exclusion mechanism the smallest polystyrene has the largest retention volume, and the polystyrene with the largest molecular weight elutes first. These peak shapes shown in Fig. 4.8 are in good agreement with the literature, where it was demonstrated that peak shapes strongly depend on the molecular size relative to the pore size [84]. Here the red dashed lines show symmetrical peaks because the molecules are small enough to enter the pores, while excluded molecules and the ones that are just below the exclusion limit form the asymmetrical blue profiles.

BACSKAY, I., **SEPSEY, A.**, FELINGER, A., Determination of the pore size distribution of high-performance liquid chromatography stationary phases via inverse size exclusion chromatography, J. Chromatogr. A, 2014, 1339, 110–117.

To determine the pore shape, first we assumed uniform pore size (monopore structure). In Fig. 4.9 the distribution coefficient is plotted against the the size parameter, ρ and Eq. 2.13 was fitted to the respective calculated K_{SEC} values of the polystyrenes via m, the pore geometry constant. This K_{SEC} ignores the PSD and assumes that the spherical molecules are all of the same size. We can see that for both the TPPs and the SPPs, the respective m values are between 2.14 and 3.07, so further on we assume cylindrical or conical/spherical pores.

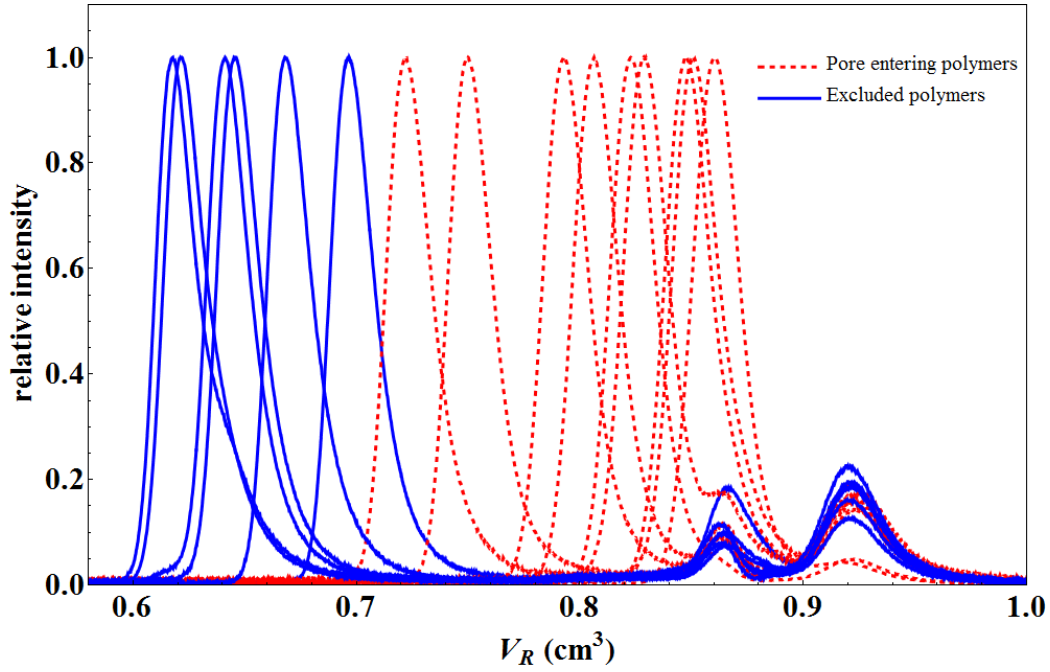

Fig. 4.8: Superposition of SEC chromatograms obtained with polystyrene standards on a Phenomenex Aeris Widepore column. Red (dashed) and blue (solid) lines indicate the molecules that can enter the pores and the molecules that are excluded form the pores, respectively.

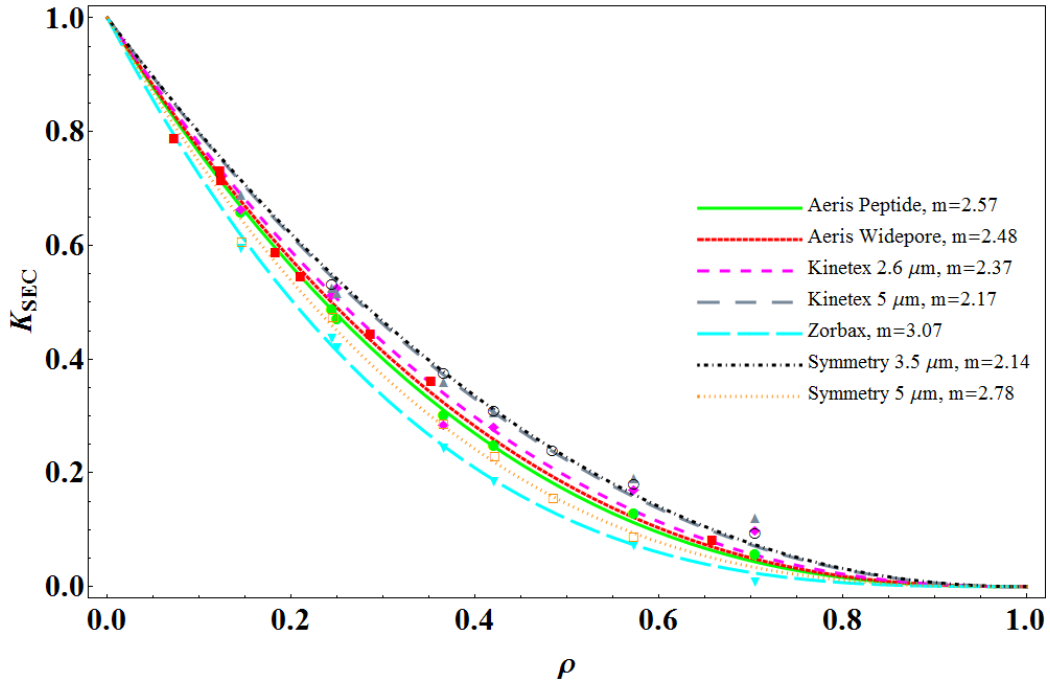

Fig. 4.9: Exclusion curves of various HPLC columns ignoring the PSD; K_{SEC} and ρ were calculated using Eq. 2.6 and Eq. 2.12, respectively. Eq. 2.13 is fitted via m to the calculated K_{SEC} values.

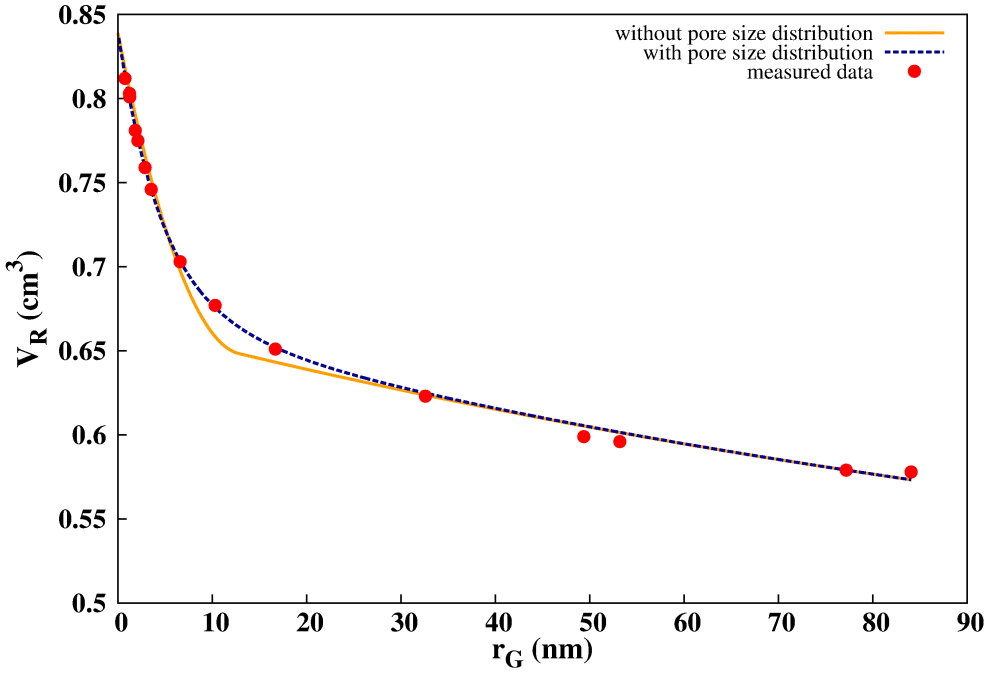

Fig. 4.10: SEC calibration curve obtained on a Phenomenex Aeris Widepore column. V_R is corrected for the extra-column volume; r_G is calculated using Eq. 2.10

Traditionally the plot of the logarithm of the molecular weight versus the retention volume (log M_W vs. V_R) is called as the calibration curve in SEC (as shown in Fig. 2.6) that shows the accessibility of the stationary phase to samples. However the molecular weight is related to the gyration radius of the molecules (see Eq. 2.10) and by plotting V_R against r_G, we easily can obtain the void volume (the volume of mobile phase to load the column, V_0), the pore volume (V_p) and the pore size (r_p) by nonlinear fitting of Eq. 2.7 using Eq. 2.13 to the retention data of the polystyrene standards. This is shown in Fig. 4.10 with solid orange line for data obtained on a Phenomenex Aeris Widepore column. The obtained results of the same fitting procedure for the other columns used in this study are listed in Table 4.1 for cylindrical ($m = 2$) and conical/spherical ($m = 3$) geometry assumed.

A Fisher test was performed to compare the variance of residuals (χ^2) of the fittings. There are no significant differences at 5% significance level between the goodness of fit (the F values are between 1.28 and 2.74, $F_{\text{critical}} = 2.98$), while assuming cylindrical and conical pore shape.

Tab. 4.1: Parameters obtained for the monopore model in case of cylindrical ($m = 2$) and conical/spherical pores ($m = 3$); V_0, V_p, and r_p were obtained by nonlinear fitting of Eq. 2.7

	m=2				m=3			
Column	V_0 (cm^3)	V_p (cm^3)	r_p (nm)	χ^2	V_0 (cm^3)	V_p (cm^3)	r_p (nm)	χ^2
Aeris Peptide	0.682±0.002	0.221±0.009	5.757±0.295	5.058×10^{-5}	0.682±0.002	0.231±0.009	7.627±0.372	3.622×10^{-5}
Aeris Widepore	0.666±0.002	0.158±0.005	14.666±0.961	4.472×10^{-5}	0.666±0.002	0.162±0.004	19.527±1.094	2.725×10^{-5}
Kinetex 2.6 µm	0.690±0.003	0.226±0.011	5.389±0.319	7.404×10^{-5}	0.690±0.003	0.239±0.012	7.027±0.415	5.790×10^{-5}
Kinetex 5 µm	0.698±0.001	0.220±0.011	6.375±0.441	8.392×10^{-5}	0.698±0.001	0.224±0.010	8.777±0.576	6.101×10^{-5}
Zorbax	0.680±0.002	0.234±0.010	5.097±0.255	5.777×10^{-5}	0.680±0.002	0.249±0.011	6.609±0.324	4.302×10^{-5}
Symmetry 3.5 µm	0.502±0.004	0.238±0.004	4.980±0.068	3.241×10^{-6}	0.502±0.004	0.261±0.004	6.350±0.068	1.489×10^{-6}
Symmetry 5 µm	0.954±0.002	0.427±0.010	4.429±0.091	3.996×10^{-5}	0.954±0.002	0.454±0.019	5.724±0.225	1.094×10^{-4}

Tab. 4.2: Parameters obtained for the stochastic model with wide PSD in case of cylindrical ($m = 2$) and conical/spherical pores ($m = 3$); V_p, $r_{p,0}$ and σ were obtained applying a non-linear fitting of Eq. 2.7 with the novel formula of K_{SEC}, Eq. 4.10.

	m=2				m=3			
Column	V_p (cm^3)	$r_{p,0}$ (nm)	σ	χ^2	V_p (cm^3)	$r_{p,0}$ (nm)	σ	χ^2
Aeris Peptide	0.266±0.008	4.671±0.189	0.696±0.045	2.845×10^{-6}	0.320±0.029	5.665±0.835	0.965±0.119	1.303×10^{-5}
Aeris Widepore	0.168±0.003	12.434±0.428	0.603±0.059	4.939×10^{-6}	0.169±0.003	17.089±0.588	0.527±0.067	4.868×10^{-6}
Kinetex 2.6 µm	0.263±0.026	4.657±0.572	0.567±0.164	4.509×10^{-5}	0.268±0.027	6.287±0.786	0.509±0.188	4.561×10^{-5}
Kinetex 5 µm	0.269±0.010	5.042±0.272	0.817±0.054	3.883×10^{-6}	0.273±0.010	6.842±0.384	0.778±0.060	4.165×10^{-6}
Zorbax	0.282±0.021	4.158±0.394	0.635±0.105	1.700×10^{-5}	0.289±0.023	5.573±0.558	0.594±0.119	1.797×10^{-5}
Symmetry 3.5 µm	0.241±0.018	5.089±0.290	0.187±0.217	1.844×10^{-5}	0.258±0.016	6.597±0.336	0.121±0.317	7.100×10^{-6}
Symmetry 5 µm	0.477±0.018	4.203±0.132	0.325±0.057	4.526×10^{-6}	0.495±0.023	5.571±0.212	0.196±0.131	5.823×10^{-6}

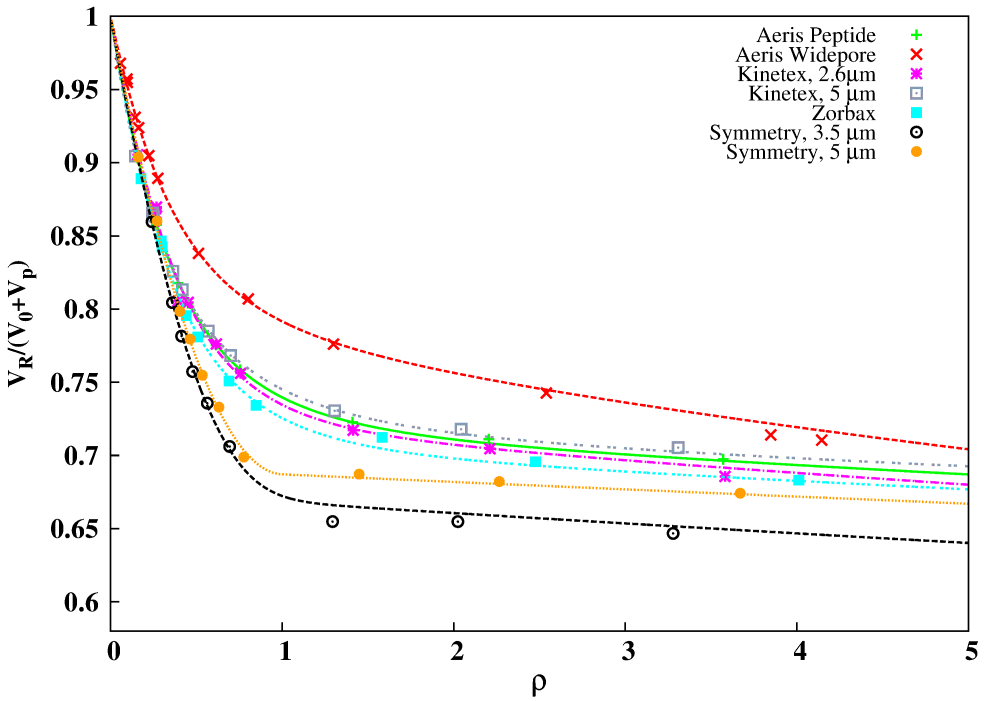

Fig. 4.11: Normalized exclusion curves obtained for various HPLC columns when the pore size distribution is considered. V_R is corrected for the extra-column volume; V_0 and V_p obtained from Table 4.2; ρ is calculated using Eq. 2.12.

As we already know, this monopore structure is not valid for the modern porous stationary phases which exhibit a rather wide PSD. To obtain the void volume, V_0, the pore volume, V_p, the mean pore size, $r_{p,0}$ and the breadth of the PSD, σ from experimental data, we should fit Eq. 2.7 combining with the K_{SEC} derived in the novel model (Eq. 4.10). The fitting is shown for the data obained with a Phenomenex Aeris Widepore column in Fig. 4.10 with blue dashed line. The obtained numerical results of this fitting are listed in Table 4.2 for the columns used in this study. The Fisher test, performed as above, shows no significant differences (the calculated F values are between 1.01 and 1.10 while the $F_{critical}$ is 3.18 at 5% significance level) between the fitted models whether cylindrical or conical pore shapes were assumed. We should note that the V_0 values obtained were the same as for the monopore model because the interstitial volume of the column and its estimation is unaffected by the PSD.

By comparing the monopore model of SEC with the model assuming wide PSD and cylindrical pore shape (Fig. 4.10), we can see and Fisher test also proves that the goodness of fit is significantly better at 5% significance level in the latter case (F = 3.40 to 21.61, $F_{critical}$ = 2.85).

Tab. 4.3: Numerical comparison of the pore size distributions calculated with the stochastic and with the Knox model with the pore size given by manufacturers; $r_{p,0}$ is the mean and σ is the standard deviation of the distribution, μ_{1,r_p} real mean pore radius (obtained usind Eq. 4.4). Data is presented in nanometers.

Column	Stochastic model			Knox model		
	$r_{p,0}$	σ	μ_{1,r_p}	$r_{p,0}$	σ	μ_{1,r_p}
Aeris Peptide	4.671	0.696	5.951	6.282	0.748	8.310
Aeris Widepore	12.434	0.603	14.913	14.977	0.653	18.536
Kinetex 2.6 µm	4.657	0.567	5.469	5.427	0.601	6.501
Kinetex 5 µm	5.042	0.817	7.040	8.045	0.870	11.746
Zorbax	4.158	0.635	5.087	5.228	0.668	6.535
Symmetry 3.5 µm	5.089	0.187	5.180	4.622	0.230	4.746
Symmetry 5 µm	4.203	0.325	4.431	4.052	0.351	4.309

Fig. 4.11 shows the normalized exclusion curves of the investigated columns where the novel model is fitted to measured data. The fitted curve of the Aeris Widepore column differs the most from the others because this type of particle has the largest pore size among the investigated ones. We can draw interesting conclusions while comparing the data obtained for the pore sizes by fitting (Tables 4.1 and 4.2) and the data given by the manufacturers (see Section 3). The Aeris Widepore column is marketed as having average pore radius of 10 nm, while the other columns are marketed having average pore radius of 5 nm (except Zorbax column with r_p =4.75 nm). The calculated pore size values are in good concordance with that of the manufacturer's data except for the Aeris Widepore column, where the closest derived value is 12.434 nm which is obtained for cylindrical pore shape. We can see that the calculated r_p values are higher for conical pore geometry.

The curves in Fig 4.11 except for Aeris Widepore column run together as long as the hindered diffusion of the polystyrenes is not considerable in the pores. The curves obtained for the two Symmetry columns decrease the deepest due to the rather narrow PSD of those stationary phases.

To prove the correctness of the stochastic model of SEC using wide PSD, we applied the often used PSD model developed by Knox et al. to our experimental data [8]. The comparison of the results obtained with the Knox model and with the stochastic model, respectively, for the seven investigated columns is presented in Fig. 4.12. One can conclude at first glance that the curves do not differ extremely, the models give similar results.

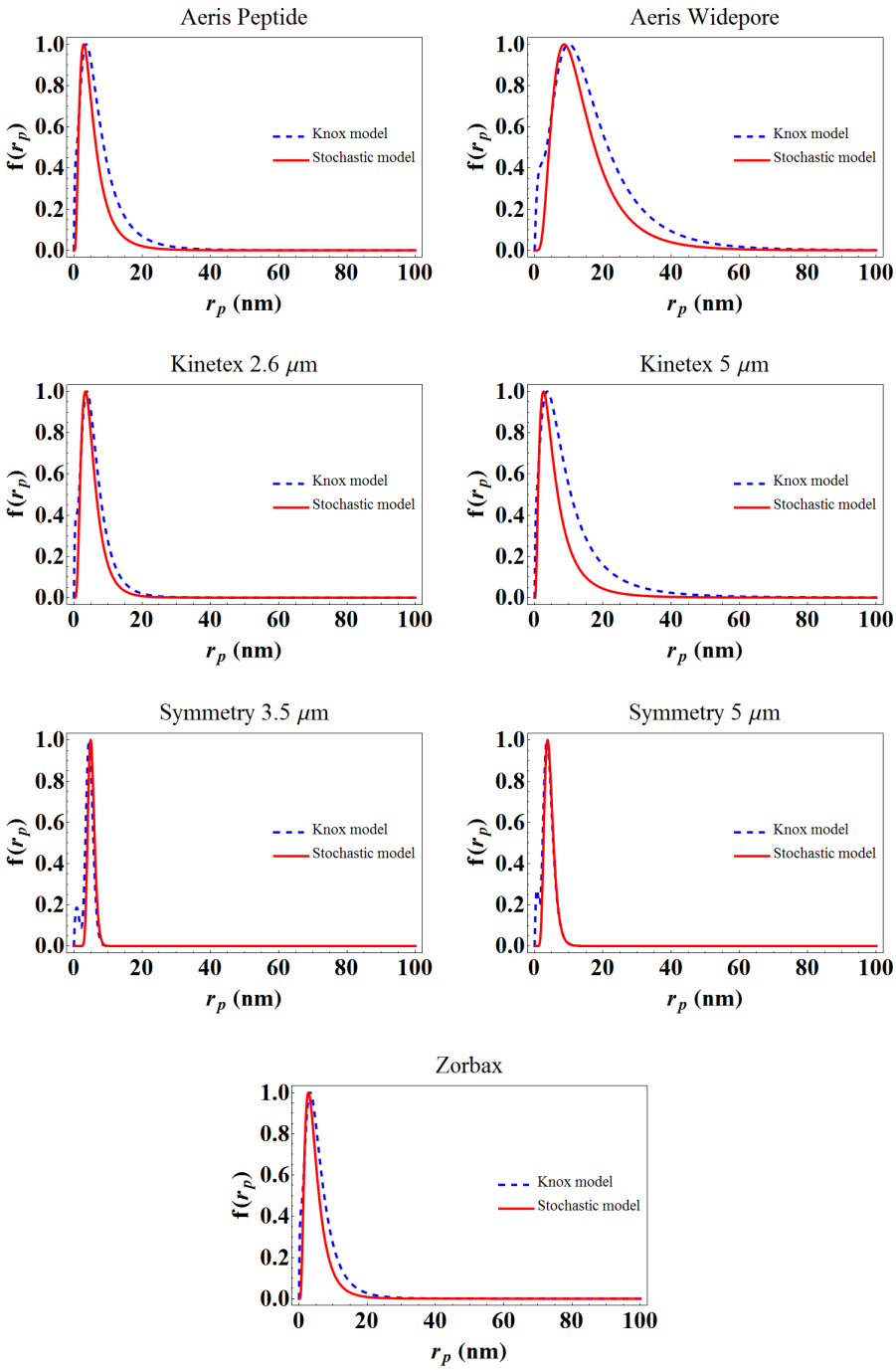

Fig. 4.12: Comparison of the results of the Knox model with those of the stochastic model with wide PSD obtained for each investigated stationary phase.

In order to go beyond simple visual comparison, we fitted the log-normal distribution (Eq. 4.3) to the data obtained with the Knox model. The numerical results are presented in Table 4.3. It can be seen that the parameters calculated with the Knox model slightly overestimate the data given by the manufacturers ($r_p = 5\,nm$, except for the Aeris Widepore column where

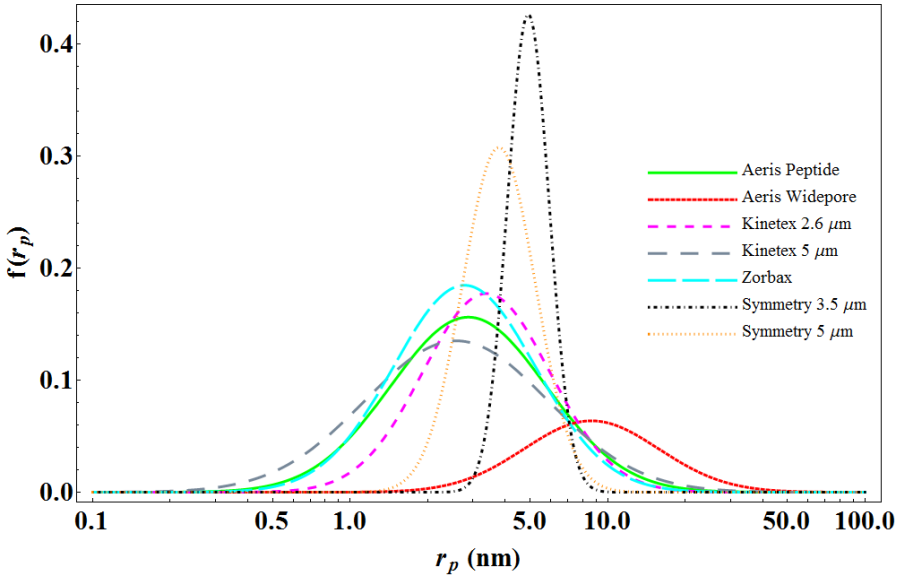

Fig. 4.13: Comparison of the pore size distribution of the various columns; pore sizes and PSDs are estimated by the stochastic theory assuming cylindrical pore shapes. $r_{p,0}$ and σ obtained from Table 4.2, substituted to Eq. 4.3.

r_p =10 nm and Zorbax column where r_p =4.75 nm). The mean of the PSD calculated using the stochastic model however slightly underestimates the manufacturers' data. Nevertheless, the agreement is rather good. These two models give much better estimations that agree more for stationary phases having narrow PSD as we can see for the Symmetry columns. We also obtained satisfactory agreement between the two approaches for the stationary phases having wider PSD. Therefore, we can conclude that Eq. 4.10 is accurate to describe K_{SEC} when the pore size exhibit a broad distribution.

It has been found by Knox et al. that the results of mercury intrusion porosimetry agree well with the estimated PSD using their SEC model. Since the currently presented stochastic theory with wide PSD yields results very similar to the Knox model, we can conclude that our model gives a rather realistic description of the structure of HPLC particles.

The difference of the pore size distribution of totally porous and superficially porous stationary phases is obvious in Fig. 4.13 where the PDFs are shown for the investigated stationary phases. The Zorbax column is an exception, because the variance of it's PSD is as high as for the SPP filled columns. The technologies to produce TPPs and SPPs are completely different. The wide PSD of superficially porous particless arise from the method of the shell synthesis [88].

4.2.2 Pore size distribution and pore geometry of monolithic columns

The novel model introduced in Section 4.1.1 allows to characterize the porous structure of the monolithic columns as well, thus we used it to determine the mesopore structure and the characteristic domain size of 1G and 2G, silica-based C_{18} monolithic HPLC columns. We carried out inverse size-exclusion experiments using the same polystyrene standards and experimental procedure as for the columns packed with totally porous particles and superficially porous particles and represented the experimental results via the molecular theory of ISEC expanded for pore size distribution.

BACSKAY, I., **SEPSEY, A.**, FELINGER, A., The pore size distribution of the first and the second generation of silica monolithic stationary phases, J. Chromatogr. A, 2014, 1359, 112–116.

Fig. 4.14 represents the calibration curves obtained with the 1G and 2G monolithic columns where the retention volumes, V_R are plotted against the gyration radius of polystyrenes, r_G. One can see that the standards that can enter the mesopores have rather similar retention volumes on both columns and the difference between the columns is more pronounced for excluded polystyrenes, i.e. in the range of hydrodynamic chromatography.

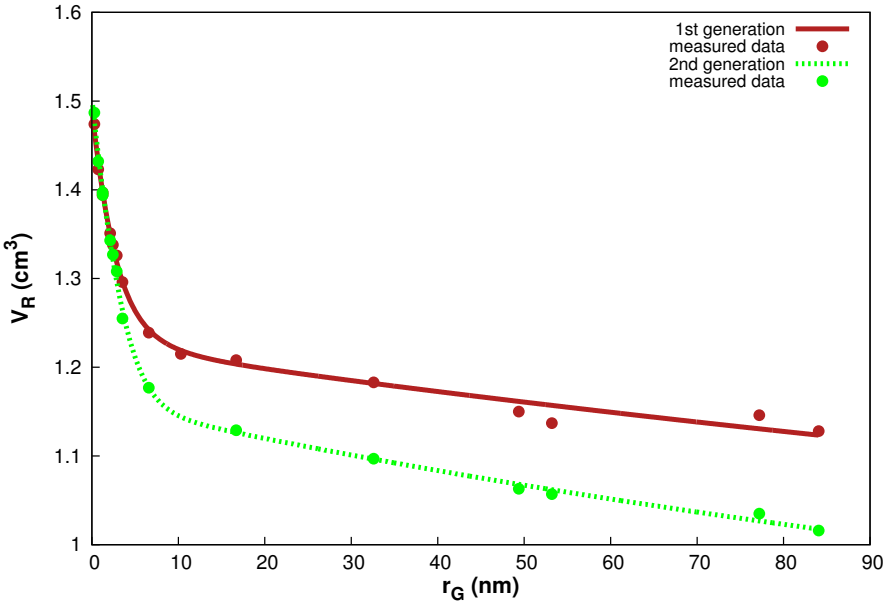

Fig. 4.14: SEC calibration curves obtained for the 1G and 2G monolithic columns. Eq. 2.7 with K_{SEC} expressed by Eq. 4.10 was fitted to the measured retention volumes via parameters V_0, r_0, V_p, $r_{p,0}$, and σ. V_R is corrected for the extra-column volume and r_G was calculated using Eq. 2.10.

Tab. 4.4: Parameters obtained by the stochastic model of SEC with wide pore size distribution. The macropore volume (V_0), the macropore radius (r_0), the mesopore volume (V_p), the mesopore radius ($r_{p,0}$), and the standard deviation of the PSD (σ) were obtained by nonlinear fitting of Eq. 2.7 with K_{SEC} expressed by Eq. 4.10. The average value of the pore radius (μ_{1,r_p}) was calculated using Eq. 4.4.

	Monolithic column	
	1G	2G
V_0 (cm^3)	1.225 ± 0.011	1.160 ± 0.007
r_0 (μm)	1.545 ± 0.280	0.949 ± 0.075
V_p (cm^3)	0.265 ± 0.007	0.343 ± 0.008
$r_{p,0}$ (nm)	7.446 ± 0.326	8.297 ± 0.318
σ	0.580 ± 0.093	0.369 ± 0.120
χ^2	3.465×10^{-5}	6.659×10^{-5}
μ_{1,r_p} (nm)	8.810	8.882

The lines in Fig. 4.14 show the results of nonlinear fitting of Eq.2.7 to the V_R vs. r_G data with K_{SEC} expressed by Eq. 4.10. The model defined by Eqs. 2.7 and 2.13 has two assumptions: the sample molecules are spherical and the mesopores are cylindrical. Parameters V_0, r_0, V_p, $r_{p,0}$, and σ were also fitted. The numerical results are listed in Table 4.4.

In case of monolithic stationary phases, V_0 and r_0 refer to the volume of macropore space and the radius of macropore, respectively. The macropore volume shifted towards a lower value, from 1.225 cm^3 to 1.160 cm^3 for 2G Chromolith column, it is a 5.3% reduction. The radii of macropores are found to be 1.55 and 0.95 μm in case of 1G and 2G monoliths, respectively. We estimated nearly 40% reduction of r_0. Our results are in good agreement with the observations of Hormann et al. who applied mercury intrusion porosimetry, scanning electron microscopy, confocal laser scanning microscopy, and numerical reconstruction of the morphology with chord length distribution method [29]. The differences between the absolute results arise from the different assumptions of characteristic distances and inaccuracy of the applied methods.

In our evaluation, we employed hydrodynamic chromatography to characterize the macropores. In hydrodynamic chromatography, the effective hydraulic radius of the macropore is the size parameter that characterizes the size of the macropores [75]. When confocal laser scanning microscopy is used to characterize the macropores, the distribution of the chord lengths

measured in the voids are determined regardless of the shapes of the macropores [29].

The increased mesopore volume, V_p (+22.7%) of the 2G Chromolith can be explained with the well described highly structured shape of the monolith [27, 29, 89]. The value of mesopore radius is changed from $r_{p,0} = 7.45$ q,nm to 8.30 nm and the standard deviation of the PSD is reduced from $\sigma = 0.58$ to 0.37 nm. The difference of PSD between the two generations of monolithic columns is obvious in Fig.4.15. The distribution of the mesopore sizes of the 1G Chromolith is broader and more asymmetrical, than that of the 2G column.

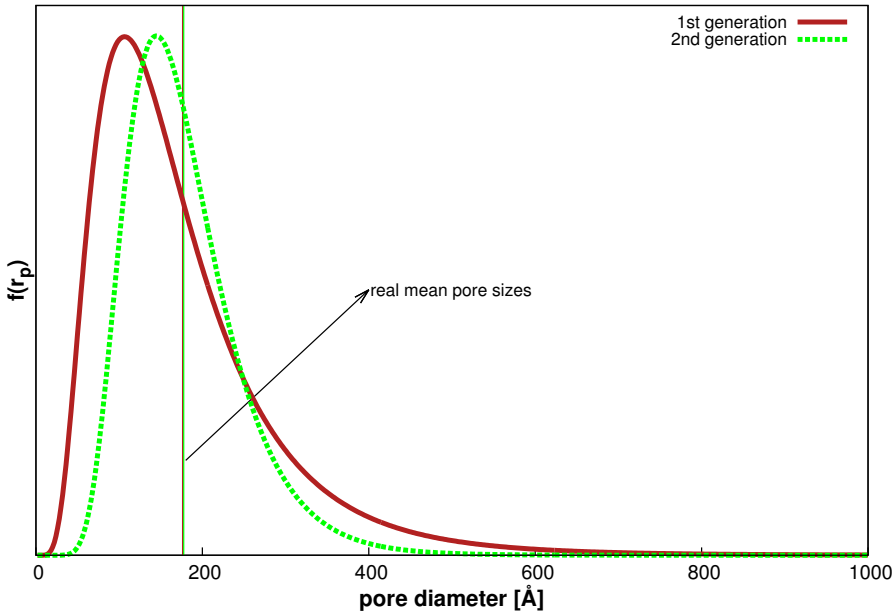

Fig. 4.15: Comparison of the PSD of the 1G and 2G monolithic columns; mesopore sizes and their distribution are estimated by the stochastic theory. $r_{p,0}$ and σ were obtained from Table 4.4 and substituted to Eq. (4.17).

The mesopore sizes determined with ISEC (14.9 nm and 16.6 nm for the 1G and 2G monoliths, respectively) are somewhat higher than the values the manufacturer reports (13 nm and 15 nm). The difference, however is insignificant, no more than 10–15%. The origin of that deviation lies most probably in the different ways of pore size determination. Each method has its own bias as pore sizes are estimated with various physical methods. Hormann et al. [29], for instance, reported 11.8 and 14.7 nm mesopore size

for the 1G and 2G monolithic columns on the basis of mercury intrusion porosimetry.

Due to the asymmetrical log-normal distribution of mesopore sizes, $r_{p,0}$ is not the real average value of the pore sizes but that can be obtained with calculation of the first moment of log-normal distribution as noted in Eq. 4.4. Practically, there is no difference between the two generations of monolithic when the real average mesopore sizes are compared (Fig. 4.15, Table 4.4), the μ_{1,r_p} values coincide.

The pore structure and morphology of the silica-based monolithic columns have been thoroughly studied with different approaches, such as mercury intrusion porosimetry, scanning electron microscopy and confocal laser scanning microscopy, etc. Our investigation has revealed that simple chromatographic experiments can also provide substantial and accurate information regarding the pore structure of monolithic columns. The combination of ISEC experiments with a proper theory can be an attractive alternative to characterize the mesopores and macropores of stationary phases with tools that are present in a chromatography laboratory.

4.3 Effect of Polydispersity

While investigating the effect of the pore size distribution on the separation in SEC, we assumed that the standard polymers are of uniform size. This, however, is not true. Even though the standards used for the calibration process have well-defined molecular weights, they do have a distribution in their molecular weight and manufacturers use a quantity to characterize the fitness-to-purpose of these polymers, polydispersity (P).

We already know that polydispersity leads to an increase in the peak width thus decreases the efficiency of the separation. This effect however can't be obtained experimentally by SEC, thus there is a need for a theoretical model to demonstrate the limitations of the contribution of polydispersity. We integrate polydispersity into the the microscopic (stochastic) theory of SEC to obtain the real contribution of polydispersity to the retention properties and efficiency.

4.3.1 Integrating polydispersity into the Stochastic Theory of Size Exclusion Chromatography

To determine the molecular weight distribution of a sample, an accurate calibration process is needed where the knowledge of the accurate molecular weight and size of the standards is of a great importance. When the size-exclusion process is described at the molecular level by the stochastic theory, polydispersity must be incorporated. This will provide a closer understanding of the influence of polydispersity and one will get a clearer picture about its consequences on the separation process and on the retention properties.

Sepsey, A., Bacskay, I., Felinger, A., Polydispersity in size-exclusion chromatography: A stochastic approach, J. Chromatogr. A, 2014, 1365, 156–163.

The concept for multiple-site adsorption can be extended for a continuous distribution of sites in adsorption chromatography as well as for a continuous distribution of pore sizes in SEC (Section 4.1.1). Following the same reasoning we can take polydispersity of the sample into account. When $\mathcal{y}$ types of molecules are present, each with a relative abundance of p_j, ($j = 1, \ldots, \mathcal{y}$), the characteristic function is then written as

$$\phi(\omega) = \exp\left\{ n_\mathrm{p} \left[\sum_{j=1}^{\mathcal{y}} p_\mathrm{j} \frac{1}{1 - i\omega\tau_{\mathrm{p,j}}} - 1 \right] \right\}, \tag{4.11}$$

where $\tau_{p,j}$ is the time spent by the jth molecule in a pore. We should note that however Eq. 4.11 looks identical to Eq. 4.1, it holds other information about the relationship of the molecules and the pores.

Eq. 4.11 can be extended to a continuous distribution of molecular sizes. Because both the pore ingress and egress processes are influenced by polydispersity, the PDF of the molecular size distribution, $\kappa(r_G, r_{G,0}, \sigma)$, should be introduced to the model. The term r_G in Eq. 2.12 and also in Eqs. 2.14 and 2.15 should be replaced by that PDF. Then the following characteristic function is derived:

$$\phi(\omega) = \exp\left[\int_0^{r_p} \kappa(r_G, r_{G,0}, \sigma) n_p(r_G) \left(\frac{1}{1 - i\omega\tau_p(r_G)} - 1\right) dr_G\right], \quad (4.12)$$

where $n_p(r_G)$ and $\tau_p(r_G)$ represent the dependence of n_p and τ_p on the gyration radius of the molecule.

Polydispersity is described by three types of distributions in the literature: Poisson, log-normal, and normal distribution. Although referring to the central limit theorem for large numbers, both the Poisson and log-normal distributions can be approximated by normal distribution; here we show the characteristic function and the derived moments for both the log-normal and normal distributions.

Log-normal distribution

The log-normal distribution of the gyration radius of the molecules is defined as

$$\kappa(r_G, r_{G,0}, \sigma)^{\log-\text{norm}} = \frac{1}{\sqrt{2\pi}\sigma r_G} \exp\left(-\frac{(\ln r_G - \ln r_{G,0})^2}{2\sigma^2}\right), \quad (4.13)$$

where $r_{G,0}$ and σ represent the mean and the standard deviation of the distribution, respectively. After substituting Eq. 4.13 into Eq. 4.12 and calculating the moments by Eq. 2.20, the following moments are derived:

$$\mu_1 = n_{perm}\tau_{perm}a_\varphi^{\log-\text{norm}}, \quad (4.14)$$

$$\mu_2' = 2n_{perm}\tau_{perm}^2 a_\varphi^{\log-\text{norm}}, \quad (4.15)$$

where $a_{\varphi}^{\log-\mathrm{norm}}$ is determined by the following expression:

$$a_{\varphi}^{\log-\mathrm{norm}} = \frac{1}{2}\sum_{k=0}^{\varphi}(-\rho)^k e^{k^2\sigma^2/2}\binom{\varphi}{k}\,\mathrm{erfc}\left(\frac{k\sigma^2+\ln\rho}{\sqrt{2}\sigma}\right), \tag{4.16}$$

where φ refers to the proper sum of m_e and m_p for the different moments and thus strongly depends on the pore geometry. For the calculation of μ_1, $\varphi = m_\mathrm{e} + m_\mathrm{p}$ should be used and if $\varphi = 1$, the pore is slit shaped, if $\varphi = 2$ it is cylindrical and if $\varphi = 3$, the pore is either conical or spherical. In this case $a_{\varphi}^{\log-\mathrm{norm}}$ is equal to K_SEC. The second central moment can be calculated using $\varphi = m_\mathrm{e} + 2m_\mathrm{p}$, and the third central moment by using $\varphi = m_\mathrm{e} + 3m_\mathrm{p}$.

Note that Eqs. 4.14 to 4.16 are identical to the ones we obtained for the size-exclusion process of monodisperse samples on stationary phase particles with log-normal PSD (see Section 4.1.1). Thus, we can conclude that PSD of the stationary phase and polydispersity have absolutely identical effect on the band profile as long as their distributions are identical. There is no way to tell their influence apart.

Normal distribution

For further calculations we use the normal distribution in this work. In case of normal distribution, the following PDF is used:

$$\kappa(r_\mathrm{G}, r_{\mathrm{G},0}, \sigma)^{\mathrm{norm}} = \frac{1}{\sqrt{2\pi}\sigma}\exp\left(-\frac{(r_\mathrm{G}-r_{\mathrm{G},0})^2}{2\sigma^2}\right), \tag{4.17}$$

where $r_{\mathrm{G},0}$ and σ represents the mean and the standard deviation of the normal distribution, respectively.

The characteristic function of the peak shape for normal PSD will be obtained by integrating Eq. 4.17 into Eq. 4.12:

$$\begin{aligned}\phi(\omega)' = \exp\Bigg[\frac{1}{\sqrt{2\pi}\sigma}\int_0^{r_\mathrm{p}} n_\mathrm{p}(r_\mathrm{G})\cdot \\ \cdot\ \exp\left(-\frac{(r_\mathrm{G}-r_{\mathrm{G},0})^2}{2\sigma^2}\right)\left(\frac{1}{1-i\omega\tau_\mathrm{p}(r_\mathrm{G})}-1\right)\mathrm{d}r_\mathrm{G}\Bigg]\end{aligned} \tag{4.18}$$

One should exercise caution when Eq. 4.18 is used, because as polydispersity increases, smaller fraction of the molecules can enter the pores. The fraction

of polymer molecules that can enter the pores should be determined by integrating the PDF of the normal distribution between the proper limits. After taking this into account, a new equation was derived for the characteristic function:

$$\phi(\omega) = (1-\epsilon) + \epsilon \exp\left[\frac{1}{\sqrt{2\pi}\sigma}\int_0^{r_\mathrm{p}} n_\mathrm{p}(r_\mathrm{G}) \cdot \right.$$
$$\left. \cdot \exp\left(-\frac{(r_\mathrm{G}-r_{\mathrm{G},0})^2}{2\sigma^2}\right)\left(\frac{1}{1-i\omega\tau_\mathrm{p}(r_\mathrm{G})}-1\right)\mathrm{d}r_\mathrm{G}\right] \tag{4.19}$$

where ϵ represents the fraction of the molecules that are small enough to enter the pores:

$$\epsilon = \frac{1}{\sqrt{2\pi}\sigma}\int_0^{r_\mathrm{p}} \exp\left(-\frac{(r_\mathrm{G}-r_{\mathrm{G},0})^2}{2\sigma^2}\right) dr_\mathrm{G} \tag{4.20}$$

Eq. 4.19 is the characteristic function of the elution profile for a polydisperse sample at any value of ρ. It contains detailed information for the separation process and the chromatogram can be calculated as its inverse Fourier transform. Eq. 4.19, however, cannot be evaluated analytically for the general case, only the calculation of the moments is possible. A simple analytical expression of the moments can only be obtained if parameters m_e and m_p are both integers, $m_\mathrm{e} > 0$ in Eq. 2.14 and $m_\mathrm{p} < 0$ in Eq. 2.15 as mentioned before for the pore size distibution.

To obtain K_SEC and the moments of a peak profile, one needs to know the size parameter, ρ and the relative standard deviation of the molecule size distribution, δ_r defined as the ratio of the standard deviation of the molecule size distribution to the mean of that distribution:

$$\delta_\mathrm{r} = \frac{\sigma}{r_{\mathrm{G},0}} \tag{4.21}$$

Subscript r in Eq. 4.21 shows that δ_r depends on the radius of the molecules.

The relation between polydispersity, P defined by Knox and the relative standard deviation of the distribution of molecular weights, δ_M is relatively simple [90]:

$$\delta_\mathrm{M}^2 = P - 1. \tag{4.22}$$

The relationship between the weight and radius of polymer molecules is defined by Eq. 2.10 and as mentioned there, the typical values for parameter

B are around $B \approx 0.5$. Therefore molecular weight is roughly proportional with the square of the molecular radius for polymers: $M_W \propto r_G^2$.

The distribution of molecular weights will be no longer normal, it will differ from the distribution of the radii. Monte Carlo simulation by generating one million normally distributed random numbers was carried out. The simulation shows that a relationship $\delta_M \approx 2\delta_r$ can be established. Thus, polydispersity is related to the size distribution of the molecules as

$$4\delta_r^2 \approx P - 1. \tag{4.23}$$

The moments of the elution profile will be obtained from Eq. 4.18. They are similar to the moments obtained for log-normal distribution (see Eqs. 4.14 – 4.15), but only if all the molecules can enter the pores, i.e. if $\epsilon \approx 1$. In this case the following equations can be used:

$$\mu_1 = n_{perm}\tau_{perm}a_\varphi^{norm}, \tag{4.24}$$

$$\mu_2' = 2n_{perm}\tau_{perm}^2 a_\varphi^{norm}, \tag{4.25}$$

where a_φ^{norm} strongly depends on the molecular size and on the pore shape and its expression becomes more complex as m increases.

Parameter a_φ^{norm} depends on which moment is being calculated and on the pore geometry, thus on the value of m_e and m_p. For the sake of brevity, we introduce the normalized variable

$$\psi = \frac{1-\rho}{\sqrt{2}\delta_r\rho} \tag{4.26}$$

a_0^{norm} is used if $m = m_e + m_p = 0$ in μ_1, or if $m_e + 2m_p = 0$ in μ_2'.

$$a_0^{norm} = \frac{1}{2}\mathrm{erfc}\,(-\psi) \tag{4.27}$$

a_1^{norm} is used if $m = m_e + m_p = 1$ in μ_1, or if $m_e + 2m_p = 1$ in μ_2'.

$$a_1^{norm} = \frac{1-\rho}{2}\left[\mathrm{erfc}\,(-\psi) + \frac{1}{\sqrt{\pi}\psi}\exp\left(-\psi^2\right)\right] \tag{4.28}$$

a_2^{norm} is used if $m = m_e + m_p = 2$ in μ_1, or if $m_e + 2m_p = 2$ in μ_2'.

$$a_2^{\text{norm}} = \frac{(1-\rho)^2}{2}\left[\frac{2\psi^2+1}{2\psi^2}\operatorname{erfc}(-\psi) + \frac{1}{\sqrt{\pi}\psi}\exp\left(-\psi^2\right)\right] \tag{4.29}$$

a_3^{norm} is used if $m = m_e + m_p = 3$ in μ_1, or if $m_e + 2m_p = 3$ in μ_2'.

$$a_3^{\text{norm}} = \frac{(1-\rho)^3}{2}\left[\frac{2\psi^2+3}{2\psi^2}\operatorname{erfc}(-\psi) + \frac{\psi^2+1}{\sqrt{\pi}\psi^3}\exp\left(-\psi^2\right)\right] \tag{4.30}$$

Although a_φ^{norm} and thus the moments of the band profile can only be calculated analytically when $m_e + m_p > 0$ for μ_1 or $m_e + 2m_p > 0$ for μ_2. Nevertheless, one can always obtain the elution profile numerically with the inverse Fourier transform of Eq. 4.18 and calculate the moments by numerical integration of the peak profile.

The effect of polydispersity becomes more complicated as the size ratio exceeds above $\rho = 0.5$. In this case ϵ is getting smaller than 1, and a_φ^{norm} can not be used any more. The reason for this is that a fraction of the molecules is excluded from the pores and elutes as a split peak. Thus, new equations were derived for the first absolute and for the second central moments that incorporate the effect of ϵ. For μ_1 this means only a multiplication by ϵ. For the calculation of μ_2', the solution is not so simple. The extension of these equations to the split-peak scenario is beyond the scope of this dissertation. The equations shown above do not include the impact of the fraction of the molecules that cannot enter the pores, i.e. they consider only the cases where split peak are not observed; $\rho < 0.6$ (see Fig. 2).

4.3.2 Graphical demonstration of the novel model

The molecular model of chromatography and polydispersity described by normal distribution was used to show the effect of polydispersity on the retention properties in SEC. To properly understand the effect of polydispersity, all parameters that have impact on the band profile have to be taken into account. Thus, we calculated chromatograms by inverse Fourier transform for various parameter combinations to observe the caused effects.

For a monodisperse sample $P = 1$, while for a narrowly distributed standard $P = 1.05$ is a typical pre-estimate. According to the Monte Carlo simulation this latter polydispersity corresponds to $\delta_r = 0.113$, which is a moderately

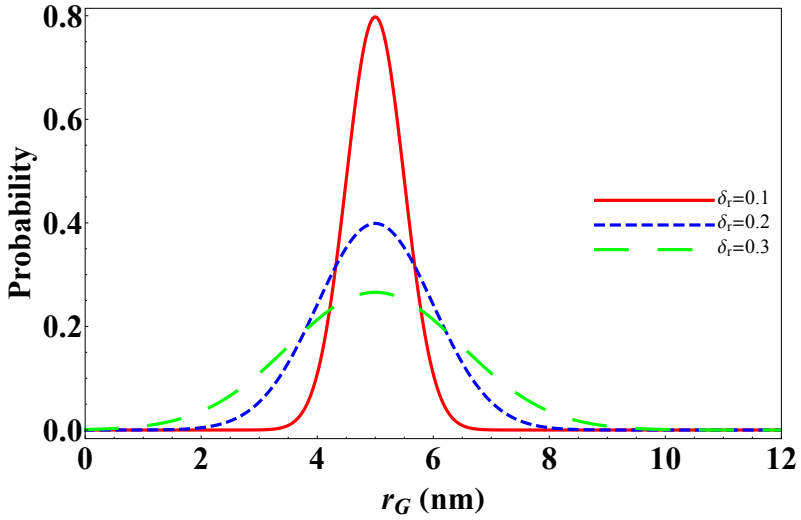

Fig. 4.16: Effect of the relative standard deviation of the molecule size distribution (polydispersity), δ_r on the size distribution of the sample molecules. The average molecule size was set to 5 nm and the individual curves represent the percentage probability of the molecule sizes if δ_r is 0.1, 0.2 and 0.3, respectively.

broad distribution. In Fig. 4.16, the effect of the relative standard deviation, δ_r on the distribution of the size of the sample molecules is shown. The average molecule size was set to $r_G = 5$ nm and the individual curves represent the percentage probability of the molecule sizes if $\delta_r = 0.1$, 0.2 and 0.3. It can be concluded that even a narrow distribution has a large impact on the molecular size. If δ_r were set to zero, all the molecules would be of the same size and we would only see a high pulse at 5 nm. In the present study, the effect of polydispersity will not be investigated for $\delta_r > 0.3$, which value corresponds to $P = 1.32$ according to the Monte Carlo simulation. Furthermore, Fig. 4.16 confirms that when $\delta_r > 0.3$, a significant part of the the distribution would span to negative sizes and the model would lose its physical background.

Table 4.5 summarizes the δ_r values calculated using Eq. 4.23 for various polydispersities. It can be seen that these values are in good agreement with the ones obtained via the Monte Carlo simulation.

As polydispersity increases, a fraction of the molecules will be excluded from the pores, since the distribution will span beyond the pore size and the characteristic function that considers partial exclusion is given in Eq. 4.19. The fraction of the molecules that can actually enter the pores (ϵ) may significantly drop if $\rho > 0.5$, depending the value of polydispersity. This

Tab. 4.5: Relative standard deviation values calculated according to the polydispersity, P using Eq. 4.23 and Monte Carlo simulation, respectively.

P	δ_r (Eq. 24)	δ_r (MC)
1.00	0	0
1.05	0.112	0.113
1.10	0.158	0.162
1.15	0.194	0.199
1.20	0.224	0.233
1.25	0.250	0.263
1.30	0.274	0.291

effect is shown in Fig. 4.17. Every single line represents the percentage of the molecules that can enter the pore at the given value of ρ for the range $0 < \delta_r < 0.3$. For the other values of ρ, $(0 < \rho < 0.5)$, ϵ is essentially equal to 1.

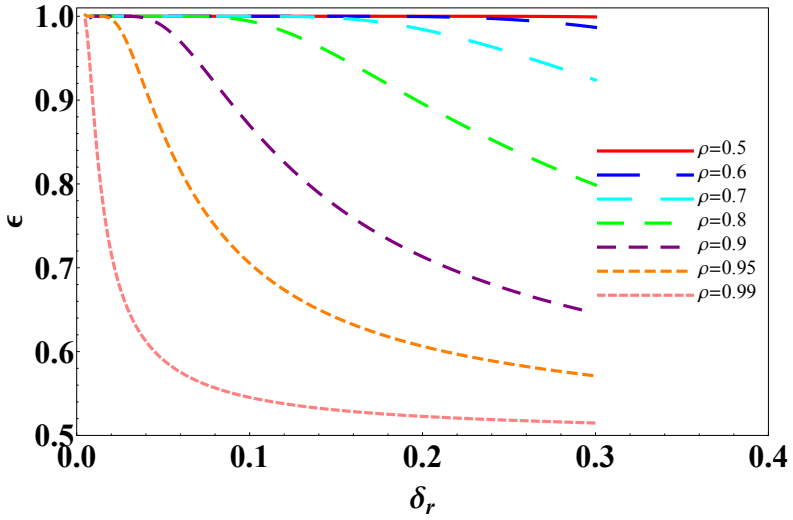

Fig. 4.17: The dependence of parameter ϵ on the relative standard deviation of the molecule size distribution (polydispersity), δ_r and on the ratio of the gyration radius of the sample molecule to the pore size, ρ. At the proper values of ρ, only the shown percentage of molecules can enter the pores.

Figure 4.18 shows the effect of polydispersity on the partition coefficient at various pore geometries. This can be achieved by depicting the four a_φ^{norm} functions (see Eqs. 28-31 in Appendix) in case of $\varphi = 1$, when the obtained expression is equal to K_{SEC}. In Fig. 4.18.a, $m = 0$, so no geometry is assumed. It can be seen that in the near monodisperse case ($\delta_r = 0.01$) there is a sharp step at $\rho = 1$. This means that the molecules that are smaller than the pore

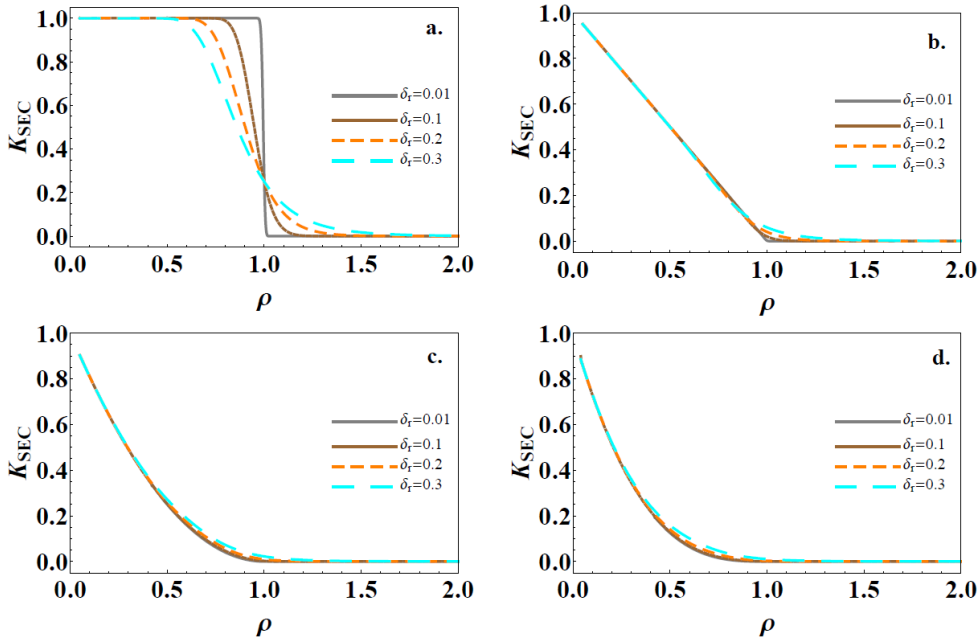

Fig. 4.18: The effect of the relative standard deviation of the molecule size distribution (polydispersity) (δ_r) and the size of the molecule relative to the pore size (ρ) on the partition coefficient (K_{SEC}) at various pore geometries. a; the pore geometry is not included ($m = 0$ i.e. relative pore accessibility), b; slit shaped pores ($m = 1$), c; cylindrical pores ($m = 2$) and d; conical or spherical pores ($m = 3$).

size can enter the pores while the molecules that are larger than the pores are all excluded. This sharp division gets blurred as we increase the value of δ_r, because there will be molecules that are either smaller or larger than the average molecule. These molecules behave differently because of their size. The same effect can be seen in Figs. 4.18.b, to 4.18d where slit shaped, cylindrical and conical or spherical pore shapes are expected, respectively. The exclusion limit tends to decrease as the pore geometry becomes more complex.

Usually, it is assumed that polydispersity does not affect the retention time (the first absolute moment) of the band profile, and only its band-broadening effect is studied. Fig. 4.19 demonstrates the effect of the relative standard deviation of the molecular size, δ_r on the chromatogram and on its first absolute and second central moments. The ratio of the molecule size to the pore size was $\rho = 0.5$ thus all the molecules can enter the pores according to Fig. 4.17 in the investigated range of δ_r. It can be noticed that – in contrast to general beliefs – the increase in polydispersity leads to a shift of retention time (except for $m = 1$) and also causes band-broadening.

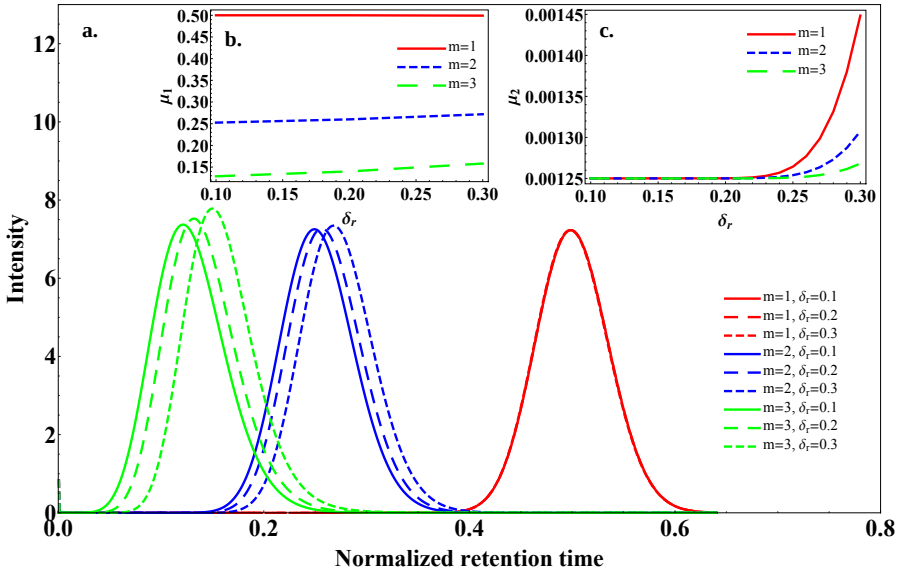

Fig. 4.19: The effect of the relative standard deviation of the molecule size distribution (polydispersity), δ_r on the calculated chromatograms for slit shaped pores, for cylindrical pores and for spherical or conical pores when the size parameter is $\rho = 0.5$. In the inserts the first absolute moment and the second central moments of the chromatograms are plotted. Parameters used for the calculations: $n_{perm} = 1600$, $\tau_{perm} = 1$, $\alpha = -1$.

The extent of retention time shift and band-broadening is increasing with the value of the pore geometry constant (m), thus with the complexity of the pore geometry. The chromatograms calculated for slit shaped pores have relatively high retention time and peak width compared with the other geometries. Therefore, we can conclude that the higher the complexity of the pore geometry the more efficient the separation is.

The effect of the size ratio parameter, ρ on the chromatograms, as well as on their first absolute and second central moment can be seen in Fig. 4.20. Classical SEC behavior and properties are present: by increasing parameter ρ, the molecules are more excluded from the pores and are eluted sooner. Because our model contains no other effect than polydispersity, we can say, that the effect is significant. The observed trend in the second central moments is because of the excluded ratio of the molecules appear at zero time as a Dirac delta. The farther the observed peaks are from zero, the more their second central moment changes because of the contribution of ϵ; for slit shaped pores ($m = 1$) one can see a high broadening in the range $0.6 < \rho < 0.8$ and a quick decay to $\rho = 1$. For $m = 2$ and $m = 3$, the observed peaks are near to the Dirac delta so we perceive band constriction.

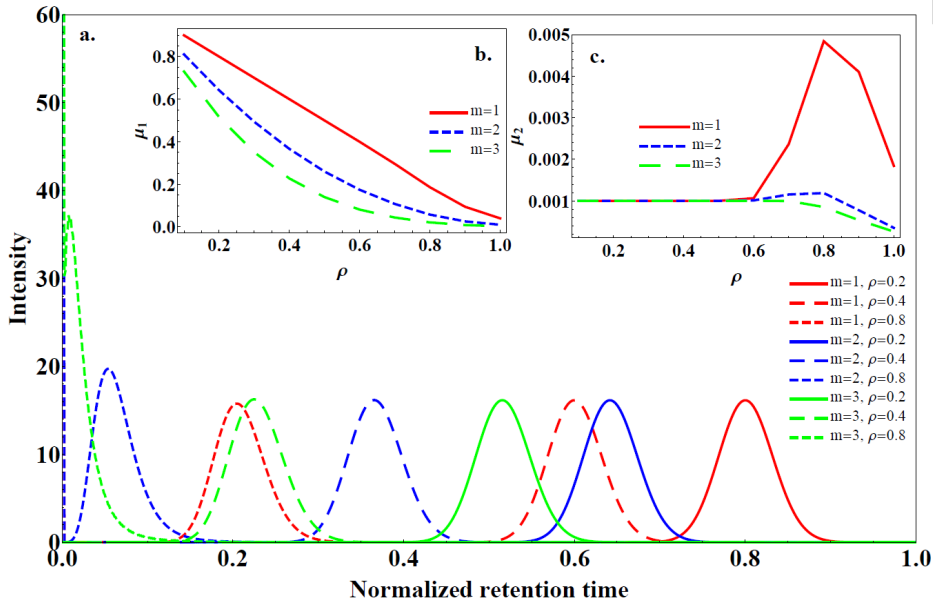

Fig. 4.20: The effect of the size parameter (ρ) on the calculated chromatograms for slit shaped pores, for cylindrical pores and for spherical or conical pores when $\delta_r = 0.2$. In the inserts the the first absolute moment and the second central moment of the chromatograms are plotted. Parameters used for the calculations: $n_{perm} = 2000$, $\tau_{perm} = 0.4$, $\alpha = -1$.

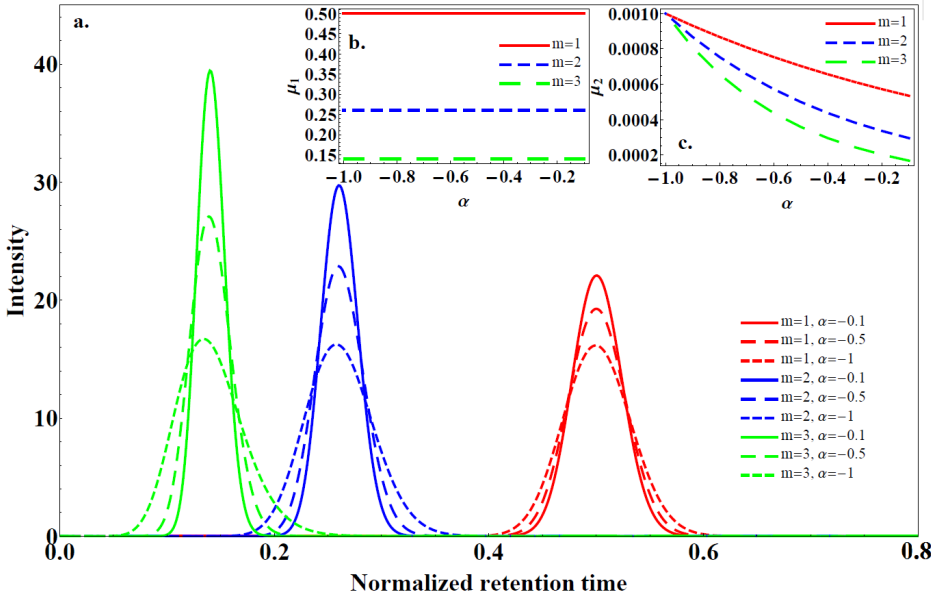

Fig. 4.21: The effect of the relative contribution of the pore egress process to the overall size-exclusion effect (α) on the calculated chromatograms for slit shaped pores, for cylindrical pores and for spherical or conical pores when $\rho = 0.5$ and $\delta_r = 0.2$. In the inserts the first absolute moment and the second central moment of the chromatograms are plotted. Parameters used for the calculations: $n_{perm} = 2000$, $\tau_{perm} = 0.4$, $\alpha = -1$.

In Fig. 4.21, the effect of the relative contribution of the pore egress process to the overall size-exclusion effect (α) on the chromatograms and on their first absolute and second central moments are showed. By calculating these, we used $\delta_r = 0.2$ and $\rho = 0.5$. The first absolute moments of the peaks do not change for the individual pore geometries. As the egress processes come to the foreground, the band-broadening becomes more significant. Similarly to the other cases presented earlier, the alteration can be best observed for the conical or spherical pore shapes.

5 Conclusion

> *Challenges are what make life interesting;*
> *overcoming them is what makes life meaningful.*
>
> — **Joshua J. Marine**

The stochastic theory of Size Exclusion Chromatography (SEC) was extended for log-normal pore size distribution (PSD) and for polydisperse samples where the molecule size is described by a normal and log-normal distribution. By assuming a pore geometry (slit shaped, cylindrical, and conical or spherical), the statistical moments of the peak profiles can easily be calculated using the derived equations and the representation of the chromatograms is feasible by inverse Fourier transform of the characteristic functions.

The results presented for the calculated chromatograms verify previous observations and experiences: both the PSD and the polydispersity have strong influence on the retention properties (retention time, peak width, and peak shape) of macromolecules. We can conclude that for the separation of macromolecules, the wide PSD will increase retention and efficiency. Therefore in all modes of liquid chromatography, the efficient separation of macromolecules calls for a broad PSD.

The novel model accounting for PSD is usable to develop SEC measurements and so to obtain relevant information from the pore structure by a non-destructive way in basis of containing information about both the pore geometry and the distribution of the pore sizes.

By using our newly developed model, Inverse Size Exclusion Chromatography has become a more accurate method to investigate the structure of a porous HPLC packing material (pore size and its distribution) without destroying the column than it was before. The stochastic theory of SEC with PSD was used to calculate the pore sizes and PSD of various commercially available HPLC columns; four of them were packed with superficially porous particles

and three were packed with totally porous particles. The novel model of SEC fits significantly better to the experimental results than the monopore model for all the columns investigated. By this fittings, we can get a realistic view of the structure of stationary phases and choose the most appropriate column to separate a complex sample.

The stochastic theory of SEC extended for log-normal PSD was used to estimate the pore size and the pore size distribution of the 1G Chromolith Performance and the 2G Chromolith High Resolution monolithic columns via Inverse Size Exclusion Chromatography. One can observe a significant difference between the SEC calibration curves of these two monolithic columns. The slopes of the curves are entirely different in the hydrodynamic range, i.e. for the molecules excluded from the mesopores. From the hydrodynamic effect, the sizes of the macropores were determined. The macropore sizes were found to be r_0 = 1.55 and 0.95 μm in case of 1G and 2G monoliths, respectively. The 22.7% increase of mesopore volume can be attributed to the highly structured macropore and skeleton structure of 2G monoliths. Although the distribution of the mesopore sizes of the 1G and 2G stationary phases differ, the real mean radii of the mesopores are similar: 8.8 and 8.9 nm, respectively.

6 Thesis points

1. The stochastic theory of Size Exclusion Chromatography was extended for log-normal pore size distribution. Chromatograms and their statistical moments were calculated by the novel model assuming certain pore geometries.

2. The parameters affecting the retention properties were changed individually to investigate their effect. It was shown that the effect of the model parameters studied (ρ, σ, α) and that of the quantities characterizing the separation (N, relative resolution) are the most intensive in case of conical pore geometry. The pore size distribution has minor influence on the retention properties of small molecules compared to the larger molecules.

3. The novel model was used to ascertain the pore size distribution and the pore geometry of various porous, spherical HPLC packing materials. The fitting of our model is in better concordance with the experimental data of non-destructive ISEC measurements compared to the model where no pore size distribution was assumed. It was confirmed that the pore size distribution of superficially porous particles packed columns is always broader compared to the totally porous particles packed columns which arise from the synthesis method.

4. The mesopore size and the pore size distribution of the two monolith generations were determined with ISEC measurements of polystyrene standards on 1G Chromolith Performance and the 2G Chromolith High Resolution monolithic columns. It was concluded that although the pore size distribution of the 2G monolith is narrower compared to the 1G monolith, there is no difference in the average mesopore size of the two generations.

5. The stochastic theory of Size Exclusion Chromatography was extended for polydisperse samples (where the molecule size is described by

a distribution). Chromatograms and their statistical moments were calculated for several pore geometries to investigate the effect of this distribution on the retention properties. It was concluded that the increase in polydispersity leads to a shift of retention time and causes band-broadening.

Acknowledgement

Immeasurable appreciation and deepest gratitude for the help and support is expressed to my supervisor Dr. Attila Felinger, who made this study possible and trusted in me throughout my work.

I owe special thanks to Dr. Ivett Bacskay for her tremendous work in the experimental part of this study, advices, valuable comments, suggestions, and last but not least for her patience.

I would like to express my gratefulness towards the colleagues of the Department of Analytical and Environmental Chemistry who all encouraged by the success of my adventure.

Immense debt of gratitude belongs to my former supervisor Dr. Krisztián Horváth, who initiated my work in the field of stochastic theory of chromatography.

Last but not least, I would like to thank my family and all of my friends their support, love and encouragement. I love you!

Publications

Publications related to this thesis

1. **Sepsey, A.**, Bacskay, I., Felinger, A., Molecular theory of size exclusion chromatography for wide pore size distributions, J. Chromatogr. A, 2014, 1331, 52–60, IF: 4.169 (Q1/D1)

2. Bacskay, I., **Sepsey, A.**, Felinger, A., Determination of the pore size distribution of high-performance liquid chromatography stationary phases via inverse size exclusion chromatography, J. Chromatogr. A, 2014, 1339, 110–117, IF: 4.169 (Q1/D1)

3. Bacskay, I., **Sepsey, A.**, Felinger, A., The pore size distribution of the first and the second generation of silica monolithic stationary phases, J. Chromatogr. A, 2014, 1359, 112–116, IF: 4.169 (Q1/D1)

4. **Sepsey, A.**, Bacskay, I., Felinger, A., Polydispersity in size-exclusion chromatography: A stochastic approach, J. Chromatogr. A, 2014, 1365, 156–163, IF: 4.169 (Q1/D1)

Posters and presentations related to this thesis

1. Bacskay, I., **Sepsey, A.**, Felinger, A., Fordított fázisú HPLC állófázisok pórusméret-eloszlása, Elválasztástudományi Vándorgyűlés 2014, 2014. 10.12–10.14., Egerszalók

2. **Sepsey, A.**, Bacskay, I., Felinger, A., Kromatográfiás állófázisok pórusméret-eloszlásnak és pórusalakjának vizsgálata, Elválasztástudományi Vándorgyűlés 2014, 2014.10.12–10.14., Egerszalók

3. Bacskay, I., **Sepsey, A.**, Felinger, A., Comparison of the pore size distribution of the two generations of silica-based monolithic stationary phases, 30th International Symposium on Chromatography, 2014.09.14–09.18. Salzburg

4. **Sepsey, A.**, Bacskay, I., Felinger, A., The effect of polydispersity in chromatography, 30th International Symposium on Chromatography, 2014.09.14–09.18, Salzburg

5. Bacskay, I., **Sepsey, A.**, Felinger, A., Comparisom of pore size distribution of RP-HPLC stationary phases with molecular theory of size-exclusion chromatography, 30th International Symposium on Microscale Bioseparations, 2014.04.27–05.01., Pécs

6. **Sepsey, A.**, Bacskay, I., Felinger, A., A Stochastic approach to the polydispersity in size exclusion chromatography, 30th International Symposium on Microscale Bioseparations, 2014.04.27–05.01., Pécs

7. **Sepsey, A.**, Bacskay, I., Felinger, A., Introducing the effect of polydispersity into the stochastic theory of size-exclusion chromatography, Interdiszciplináris doktorandusz konferencia, 2014.04.16., Pécs

8. **Sepsey, A.**, Bacskay, I., Felinger, A., Integrating the pore size distribution into the molecular theory of size exclusion chromatography, 9th Balaton Symposium on high-per-formance separation methods, 2013.09.04–09.06., Siófok

9. Bacskay, I., **Sepsey, A.**, Felinger, A., Estimation of pore size distribution of HPLC stationary phases with the molecular theory of size-exclusion chromatography, 9th Balaton Symposium on high-performance separation methods, 2013.09.04–09.06., Siófok

10. **Sepsey, A.**, Bacskay, I., Felinger, A., Molecular theory of size exclusion chromatography for wide pore size distributions, 39th international symposium on high performance liquid phase separations and related techniques (HPLC 2013), 2013.06.16–06.20., Amsterdam

11. Bacskay, I., **Sepsey, A.**, Felinger, A., Influence of wide pore size distribution in size-exclusion chromatography, 39th international symposium on high performance liquid phase separations and related techniques (HPLC 2013), 2013.06.16–06.20., Amsterdam

12. **Sepsey, A.**, Bacskay, I., Felinger, A., Introducing pore size distribution into the stochastic theory of size exclusion chromatography, 9th János Szentágothai Interdisciplinary Conference & Student Competition, 2013. 05.03–05.04., Pécs

13. **Sepsey, A.**, Bacskay, I., Felinger, A., Modeling wide pore size distributions in size exclusion chromatography, CECE 2013 10th International Interdisciplinary Meeting on Bioanalysis, 2013.04.25–04.27., Pécs

14. Bacskay, I., **Sepsey, A.**, Felinger, A., Experimental validation of the molecular theory of size-exclusion chromatography with wide pore size distribution, CECE 2013 10th International Interdisciplinary Meeting on Bioanalysis, 2013.04.25–04.27., Pécs

Publications not related to this thesis

1. Pasti, L., Marchetti, N., Guzzinati, R., Catani, M., Bosi, V., Dondi, F., **Sepsey, A.**, Felinger, A., Cavazzini, A., Microscopic models of liquid chromatography: From ensemble-averaged information to resolution of fundamental viewpoint at single-molecule level, TRAC, 2016, IF: 6.472 (Q1/D1)

2. Horváth K., **Sepsey, A.**, Hajós P., Solvent minimization in two-dimensional liquid chromatography, J. Chromatogr. A, 2015, 1378, 32–36, IF: 4.169 (Q1/D1)

3. Horváth K., Lukács D., **Sepsey, A.**, Felinger A., Effect of particle size distribution on the separation efficiency in liquid chromatography, J. Chromatogr. A, 2014, 1361, 203–208, IF: 4.169 (Q1/D1)

4. Tófalvi R., **Sepsey, A.**, Horváth K., Hajós P., Environmental significance and identification of metal-chelate complexes using ion chromatography, Hung. J. Ind. Chem., 2011, 39, 95–99, IF: 0

Posters and presentations not related to this thesis

1. **Sepsey, A.**, Felinger, A., The theory of “Batman peaks”: dinamic interconversions during the chromatographic separation, Balaton Symposium on High-Performance separation methods, 2015.09.02–09.04., Siófok

2. **Sepsey, A.**, Felinger, A., Stochastic theory of “Batman” peaks: a novel model for enantiomer separation, 15th International Symposium and Summer School on Bioanalysis, 2015.07.13–07.18., Marosvásárhely

3. **Sepsey, A.**, Felinger, A., Molecular dynamic theory of “Batman” peaks: enantiomer separation using the stochastic theory of chromatography, 42nd International Symposium on High Performance Liquid Phase Separations and Related Techniques, 2015.06.21–06.25., Genf

4. Horváth, K., **Sepsey, A.**, Hajós, P., New strategy for solvent optimisation in multi dimensional green chromatography, 1st EuCheMS Congress on Green and Sustainable Chemistry, 2013.10.13–10.15., Budapest

5. Horváth K., **Sepsey, A.**, Hajós P., Novel approaches for the optimization of off-line two-dimensional liquid chromatography, 29th International Symposium on Chromatography (ISC’2012), 2012.09.09–09.13., Torun

6. Horváth, K., **Sepsey, A.**, Lukács, D., Felinger, A., Influence of width of particle size distribution on separation efficiency in liquid chromatography, 9th Balaton Symposium on high-performance separation methods, 2013.09.04–09.06. Siófok

7. Horváth, K., **Sepsey, A.**, Hajós, P., Solvent minimization in two-dimensional liquid chromatography, 9th Balaton Symposium on high-performance separation methods, 2013.09.04–09.06. Siófok

8. **Sepsey, A.**, Horváth K., Hajós P., Az off-line kétdimenziós folyadékkromatográfia optimalizálásának újszerű megközelítése, Elválasztástudományi Vándorgyűlés 2012, 2012.11.07–11.09., Hajdúszoboszló

9. Tófalvi, R., **Sepsey, A.**, Horváth, K., Hajós, P., Simultaneous analytical separation of metal-chelate complexes and their ligands using high performance ion chromatography, 36th International Symposium on

High-Performance Liquid Phase Separations and Related Techniques (HPLC 2011), 2011.06.19–06.23., Budapest

10. Tófalvi, R, **Sepsey, A.**, Horváth, K., Hajós, P., Fémkelát komplexek és ligandumok szimultán analitikai elválasztása nagyhatékonyságú ionkromatográfiával, Elválasztástudományi Vándorgyűlés 2010., 2010.11.10–11.12., Tapolca

11. Tófalvi, R, **Sepsey, A.**, Hajós, P., Fém-kelát komplexek analitikai elválasztása és azonosítása folyadék-kromatográfiás módszerrel, Műszaki Kémiai Napok 2010 (Conference of Chemical Engineering 2010), 2010. 04.27–04.29., Veszprém

List of Symbols

Greek Symbols

α	relative contribution of the pore egress process to the overall size exclusion effect
χ^2	variance of residuals
ϵ	fraction of the molecules that are small enough to enter the pores
η	viscosity of the mobile phase
$\kappa(r_G, r_{G,0}, \sigma)^{\text{lognorm}}$	probability density function of lognormal distribution for molecule size
$\kappa(r_G, r_{G,0}, \sigma)^{\text{norm}}$	probability density function of normal distribution for molecule size
μ'_k	kth central moment
μ_k	kth absolute moment
ω	auxiliary real variable in frequency domain
$\phi(\omega)$	characteristic function
ψ	normalized variable in Eqs. 4.26–4.30
ρ	size parameter, ratio of r_G to r_p
σ^2	variance
τ_m	average elementary time spent by a molecule in the mobile phase before entering a pore

τ_{perm}	average time spent in a single pore by a completely permeable particle
τ_{p}	average elementary time spent by a molecule in a single pore
ε_{e}	external porosity of the packing material
φ	auxiliary variable to calculate moments
$\zeta(r_{\mathrm{p}}, r_{\mathrm{p,0}}, \sigma)$	probability density function of lognormal distribution for pore size
erfc	error function

Other Variables

a	parameter in Eqs. 4.7–4.9
$a_{\varphi}^{\mathrm{log-norm}}$	parameter in Eqs. 4.14–4.15
$a_{\varphi}^{\mathrm{norm}}$	parameter in Eqs. 4.24–4.25
B	exponent of the power law relating the diffusion coefficient of the polymer to the reciprocal of its molecular weight
C	constant which depends on the packing-carrier-polymer system
D	diffusion coefficient
d_{core}	diameter of the core of the stationary phase particle
d_{p}	diameter of the stationary phase particle
d_{p}	particle diameter
F	calculated value for Fisher-test
F_{critical}	critical value for the Fisher-test
i	imaginary unit
I_1	modified Bessel function of the first kind and first order
K	constant in Eq. 2.10

k_B	Boltzmann constant, 1.38×10^{-23} J/K
K_{HDC}	partition coefficient accounting for the hydrodynamic chromatography contribution
K_{SEC}	partition coefficient in SEC
m	pore geometry constant
m_e	geometry constant depending on the ingress process
M_n	number-averaged relative molecular weight
m_p	geometry constant depending on the egress process
M_W	weight-averaged relative molecular weight (molecular weight)
n_{perm}	average number of the pore ingress steps by a completely permeable particle
n_p	average number of entrapment/release of a molecule in the pores
P	polydispersity
p	relative abundance
r_0	hydraulic radius of the packing material
r_{eff}	effective size of macromolecule
r_G	gyration radius of a molecule
r_p	radius of the pore opening
T	temperature
t	time
$t_{p,perm}$	time spent by the completely permeable particles in the pores of the stationary phase particles
t_p	time spent by the investigated molecules in the pores of the stationary phase particles
V_0	void/total exclusion volume of the column is SEC
V_{excl}	volume available for the excluded particles

$V_{p,perm}$	pore volume available for the totally permeable particles
V_{perm}	column volume available for the totally permeable particles
V_p	pore volume
V_R	retention volume
V_{system}	volumetric contribution of the system

Glossary

1G first generation monoliths

2G second generation monoliths

BET Brunauer-Emmett-Teller procedure

CF characteristic function

HETP height equivalent to a theoretical plate

HILIC Hydrophilic interaction chromatography

HPLC High Performance Liquid Chromatography

ISEC Inverse Size Exclusion Chromatography

IUPAC International Union of Pure and Applied Chemistry

LTNA low temperature nitrogen adsorption

PDF probability density function

PEEK polyether ether ketone

PSD pore size distribution

SEC Size Exclusion Chromatography

SEM scanning electron microscopy

SPP superficially porous particles

TEM transmission electron microscopy

THF tetrahydrofuran

TPP totally porous particles

UHPLC Ultra-High Performance Liquid Chromatography

Bibliography

(1) Snyder, L. R.; Kirkland, J. J.; Dolan, J. W., *Introduction to Modern Liquid Chromatography*; Wiley: Hoboken, New Jersey, 2010.

(2) Ohmacht, R.; Boros, B. *Chromatographia* **2000**, *51*, S205–S210.

(3) Felinger, A.; Boros, B.; Ohmacht, R. *Chromatographia* **2002**, *56*, S61–S64.

(4) Unger, K.; Jilge, G.; Kinkel, J.; Hearn, M. *J. Chromatogr.* **1986**, *359*, 61–72.

(5) Kalghatgi, K.; Horváth, C. *J. Chromatogr.* **1988**, *443*, 343–354.

(6) Gritti, F.; Leonardis, I.; Abia, J.; Guiochon, G. *J. Chromatogr. A* **2010**, *1217*, 3819–3843.

(7) Gritti, F.; Cavazzini, A.; Marchetti, N.; Guiochon, G. *J. Chromatogr. A* **2007**, *1157*, 289–303.

(8) Knox, J. H.; Scott, H. P. *J. Chromatogr. A* **1984**, *316*, 311–332.

(9) Knox, J. H.; Ritchie, H. J. *J. Chromatogr. A* **1987**, *387*, 65–84.

(10) Yao, Y.; Lenhoff, A. M. *J. Chromatogr. A* **2004**, *1037*, 273–282.

(11) Kubin, M. *Coll. Czech Chem. Commun.* **1965**, *30*, 2900–2907.

(12) Fanali, S.; Haddad, P. R.; Poole, C. F.; Schoenmakers, P.; Lloyd, D., *Liquid Chromatography: Fundamentals and instrumentation*; Elsevier: Amsterdam, 2013.

(13) Rouquerol, F.; Rouquerol, J.; Sing, K., *Adsorption by Powders and Porous Solids*; Academic Press: New York, 1999.

(14) Unger, K. K., *Porous Silica*; Elsevier: Amsterdam, 1979.

(15) Hjertén, S.; Liao, J. L.; Zhang, R. *J. Chromatogr.* **1989**, *473*, 273–275.

(16) Svec, F.; Frechet, J. M. J. *Anal. Chem.* **1992**, *64*, 820–822.

(17) Nakanishii, K.; Soga, N. *J. Am. Ceram. Soc.* **1991**, *74*, 2518–2530.

(18) Minakuchi, H.; Nakanishi, K.; Soga, N.; Ishizuka, N.; Tanaka, N. *Anal. Chem.* **1996**, *68*, 3498–3501.

(19) Minakuchi, H.; Nakanishi, K.; Soga, N.; Ishizuka, N.; Tanaka, N. *J. Chromatogr. A* **1997**, *762*, 135–146.

(20) Minakuchi, H.; Nakanishi, K.; Soga, N.; Ishizuka, N.; Tanaka, N. *J. Chromatogr. A* **1998**, *797*, 121–131.

(21) Tanaka, N.; Kobayash, H.; Nakanishi, K.; Minakuchi, H.; Ishizuka, N. *Anal. Chem.* **2001**, *73*, 420A–429A.

(22) Tanaka, N.; Kobayashi, H.; Ishizuka, N.; Minakuchi, H.; Nakanishi, K.; Hosoya, K.; Ikegami, T. *J. Chromatogr. A* **2002**, *965*, 35–49.

(23) Ishizuka, N.; Kobayashi, H.; Minakuchi, H., et al. *J. Chromatogr. A* **2002**, *960*, 85–96.

(24) Cabrera, K. *J. Sep. Sci.* **2004**, *27*, 843–852.

(25) Gritti, F.; Guiochon, G. *J. Chromatogr. A* **2009**, *1216*, 4752–4767.

(26) Gritti, F.; Guiochon, G. *J. Chromatogr. A* **2012**, *1228*, 2–19.

(27) Hlushkou, D.; Hormann, K.; Höltzel, A.; Khirevich, S.; Seidel-Morgenstern, A.; Tallarek, U. *J. Chromatogr. A* **2013**, *1303*, 28–38.

(28) Hara, T.; Kobayashi, H.; Ikegami, T.; Nakanishi, K.; Tanaka, N. *Anal. Chem.* **2006**, *78*, 7632–7642.

(29) Hormann, K.; Müllner, T.; Bruns, S.; Höltzel, A.; Tallarek, U. *J. Chromatogr. A* **2012**, *1222*, 46–58.

(30) Cabrera, K. *LC-GC North Am.* **2012**, *30 (S4)*, 56–60.

(31) Gritti, F.; Guiochon, G. *J. Chromatogr. A* **2012**, *1238*, 77–90.

(32) Fekete, S.; Veuthey, J.-L.; Eeltink, S.; Guillarme, D. *Anal. Bioanal. Chem* **2013**, *405*, 3137–3151.

(33) Giddings, J. C., *Unified Separation Science*; John Wiley & Sons: New York, 1991.

(34) Feller, W., *An Introduction to Probability Theory and its Application*, 3rd; John Wiley & Sons: New York, 1968; Vol. I.

(35) Gritti, F.; Sanchez, C. A.; Farkas, T.; Guiochon, G. *J. Chromatogr. A* **2010**, *1217*, 3000–3012.

(36) Lapidus, L.; Amundson, N. R. *J. Phys. Chem.* **1952**, *56*, 984–988.

(37) Van Deemter, J. J.; Zuiderweg, F. J.; Klinkenberg, A. *Chem. Eng. Sci.* **1956**, *5*, 271–289.

(38) Gritti, F.; Guiochon, G. *Anal. Chem.* **2013**, *85*, 3017–3035.

(39) Gritti, F.; Leonardis, I.; Abia, J.; Guiochon, G. *J. Chromatogr. A* **2010**, *1217*, 3819–3843.

(40) Gritti, F.; Guiochon, G. *J. Chromatogr. A* **2012**, *1221*, 2–40.

(41) Halász, I.; Naefe, M. *Anal. Chem.* **1972**, *44*, 76–84.

(42) Endele, R.; Halász, I.; Unger, K. *J. Chromatogr.* **1974**, *99*, 377.

(43) Dewaele, C.; Verzele, M. *J. Chromatogr.* **1983**, *260*, 13–21.

(44) Billen, J.; Guillarme, D.; Rudaz, S.; Veuthey, J.-L.; Ritchie, H.; Grady, B.; Desmet, G. *J. Chromatogr. A* **2007**, *1161*, 224–233.

(45) Cabooter, D.; Billen, J.; Terryn, H.; Lynen, F.; Sandra, P.; Desmet, G. *J. Chromatogr. A* **2008**, *1204*, 1–10.

(46) Daneyko, A.; Höltzel, A.; Khirevich, S.; Tallarek*, U. *Anal. Chem.* **2011**, *83*, 3903–3910.

(47) Gritti, F.; Farkas, T.; Heng, J.; Guiochon, G. *J. Chromatogr. A* **2011**, *1218*, 8209–8221.

(48) Horváth, K.; Lukács, D.; Sepsey, A.; Felinger, A. *J. Chromatogr. A* **2014**, *1361*, 203–208.

(49) Wagner, B. M.; Schuster, S. A.; Boyes, B. E.; Kirkland, J. J. *J. Chromatogr. A* **2012**, *1264*, 22–30.

(50) Brunauer, S.; Emmett, P. H.; Teller, E. *J. Amer. Chem. Soc.* **1938**, *60*, 309–319.

(51) Ritter, H. L.; Drake, L. C. *Ind. Eng. Chem. Anal. Ed.* **1945**, *17*, 782–786.

(52) Guan, H.; Guiochon, G. *J. Chromatogr. A* **1996**, *731*, 27–40.

(53) Gregg, S. J.; Sing, K. S. W., *Adsorption, Surface Area and Porosity*; Academic Press: London, 1982.

(54) Giaquinto, A.; Liu, Z.; Bach, A.; Kazakevich, Y. *Anal. Chem.* **2008**, *80*, 6358–6364.

(55) Gétaz, D.; Dogan, N.; Forrer, N.; Morbidelli, M. *J. Chromatogr. A* **2011**, *1218*, 2912–2922.

(56) Kele, M.; Guiochon, G. *J. Chromatogr. A* **2002**, *960*, 19–49.

(57) Urban, J.; Jandera, P.; Schoenmakers, P. *J. Chromatogr. A* **2007**, *1150*, 279–289.

(58) Al-Massaedh, A. A.; Pyell, U. *J. Chromatogr. A* **2014**, *1325*, 247–255.

(59) Halász, I.; Martin, K. *Angew. Chem., Int. Ed. Engl.* **1978**, *17*, 901–908.

(60) Yau, W. W.; Kirkland, J. J.; Bly, D. D., *Modern Size-Exclusion Liquid Chromatography*; Wiley: New York, 1979.

(61) Knox, J. H.; McLennan, F. *Chromatographia* **1977**, *10*, 75–78.

(62) Stepto, R. F. T. *Pure Appl. Chem.* **2009**, *8*, 351–353.

(63) Bly, D. D. *J. Polym. Sci. Part A-1* **1968**, *6*, 2085–2089.

(64) Bly, D. D. *Anal. Chem.* **1969**, *41*, 477–480.

(65) Unger, K. K.; Kern, R.; Ninou, M. C.; Krebs, K.-F. *J. Chromatogr. A* **1974**, *99*, 435–443.

(66) Unger, K. K.; Kern, R. *J. Chromatogr. A* **1976**, *122*, 345–354.

(67) Heyden, Y. V.; Popovici, S.-T.; Staal, B.; Schoenmakers, P. J. *J. Chromatogr. A* **2003**, *986*, 1–15.

(68) Netopilík, M.; Podzimek, S.; Kratochvíl, P. *J. Chromatogr. A* **2001**, *922*, 25–36.

(69) Netopilík, M. *J. Chromatogr. A* **1998**, *793*, 21–30.

(70) Hagel, L.; Janson, J.-C. In *Fundamentals and Applications of Chromatography and Related Differential Migration Methods Fundamentals and Techniques Part A. Vol 51.* Heftmann, E., Ed.; Elsevier: Amsterdam, 1992; Chapter 6.

(71) Teraoka, I. *Macromolecules* **2004**, *37*, 6632–6639.

(72) Potschka, M. In *Strategies in Size Exclusion Chromatography*, Potschka, M., Dubin, P. L., Eds.; ACS: Washington, DC, 1996.

(73) Stegeman, G.; Kraak, J. C.; Poppe, H. *J. Chromatogr.* **1991**, *550*, 721–739.

(74) Pasti, L.; Dondi, F.; Van Hulst, M.; Schoenmakers, P. J.; Martin, M.; Felinger, A. *Chromatographia* **2003**, *57*, S171–S186.

(75) Stegeman, G.; Kraak, J. C.; Poppe, H. *J. Chromatogr.* **1993**, *634*, 149–159.

(76) Dondi, F.; Cavazzini, A.; Remelli, M.; Felinger, A.; Martin, M. *J. Chromatogr. A* **2002**, *943*, 185–207.

(77) Giddings, J. C.; Eyring, H. *J. Phys. Chem.* **1955**, *59*, 416–421.

(78) Carmichael, J. B. *J. Polym. Sci. Part A-2* **1968**, *6*, 517–527.

(79) Carmichael, J. B. *Macromolecules* **1968**, *1*, 526–529.

(80) Carmichael, J. B. *Polym. Prepr* **1968**, *9*, 572–577.

(81) Carmichael, J. B. *Biopolymers* **1968**, *6*, 1497–1499.

(82) Dondi, F.; Remelli, M. *J. Phys. Chem.* **1986**, *90*, 1885–1891.

(83) Cavazzini, A.; Remelli, M.; Dondi, F.; Felinger, A. *Anal. Chem.* **1999**, *71*, 3453–3462.

(84) Felinger, A.; Cavazzini, A.; Remelli, M.; Dondi, F. *Anal. Chem.* **1999**, *71*, 4472–4479.

(85) Felinger, A. *LC–GC North Am.* **2004**, *22*, 642–647.

(86) Felinger, A.; Pasti, L.; Dondi, F.; van Hulst, M.; Schoenmakers, P. J.; Martin, M. *Anal. Chem.* **2005**, *77*, 3138.

(87) Felinger, A. *J. Chromatogr. A* **2011**, *1218*, 1939–1941.

(88) Guiochon, G.; Gritti, F. *J. Chromatogr. A* **2011**, *1218*, 1915–1938.

(89) Cabooter, D.; Broeckhoven, K.; Sterken, R., et al. *J. Chromatogr. A* **2014**, *1325*, 72–82.

(90) Popovici, S.-T.; Kok, W. T.; Schoenmakers, P. J. *J. Chromatogr. A* **2004**, *1060*, 237–252.

(91) Giddings, J. C., *Dynamics of Chromatography*; Marcel Dekker: New York, 1965.

(92) Gritti, F.; Guiochon, G. *J. Chromatogr. A* **2007**, *1166*, 30–46.

(93) Gritti, F.; Guiochon, G. *J. Chromatogr. A* **2003**, *1003*, 43–72.

(94) Motokawa, M.; Kobayashi, H.; Ishizuka, N., et al. *J. Chromatogr. A* **2002**, *961*, 53–63.

(95) Carr, P.; Martire, D.; Snyder, L. *J. Chromatogr. A* **1993**, *656*, 1 –2.

(96) IUPAC *Manual of symbols and terminology, appendix 2. Part I, colloid and surface chemistry, Pure Appl. Chem.* **1972**, *31*, 578.

(97) C. Orr, J. *Powder Technology* **1969**, *3*, 117–123.

(98) Barrett, E. P.; Joyner, L. G.; Halenda, P. P. *J. Am. Chem. Soc.* **1951**, *73*, 373–380.

(99) Giddings, J.; Kucera, E.; Russel, C.; Myers, M. *J. Phys. Chem* **1968**, *72*, 4397–4408.

(100) Stegeman, G.; Oostervink, R.; Kraak, J.; Poppe, H.; Unger, K. *J. Chromatogr. A* **1990**, *506*, 547–561.

(101) Unger, K. K.; Lerk, K. D.; Wirth, H. J. In *HPLC of proteins, peptides and polynucleotides: contemporary topics and applications*, Hearn, M. T. W., Ed.; VCH: New York, 1991.

(102) Kirkland, J.; Truszkowski, F.; Jr., C. D.; Engel, G. *J. Chromatogr. A* **2000**, *890*, 3–13.

(103) Kubin, M. *J. Chromatogr.* **1975**, *108*, 1–12.

(104) Felinger, A. *J. Chromatogr. A* **2008**, *1184*, 20–41.